AFIT/GAE/ENY/93D-30

EXPERIMENTAL ANALYSIS OF HEAT TRANSFER CHARACTERISTICS AND PRESSURE DROP THROUGH SCREEN REGENERATIVE HEAT EXCHANGERS

THESIS

Jeffrey L. Wiese, Captain, USAF

AFIT/GAE/ENY/93D-30

The views expressed in this thesis are those of the author and do not reflect the official policy or position of the Department of Defense or the U. S. Government

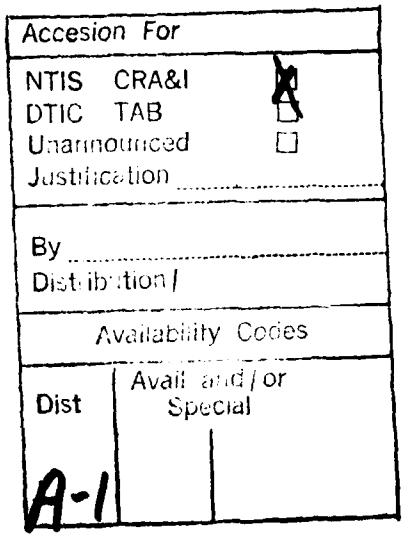

AFIT/GAE/ENY/93D-30

EXPERIMENTAL ANALYSIS OF HEAT TRANSFER CHARACTERISTICS AND PRESSURE DROP THROUGH SCREEN REGENERATIVE HEAT EXCHANGERS

THESIS

Presented to the Faculty of the Graduate School
of Engineering
of the Air Force Institute of Technology
Air University
In Partial Fulfillment of the
Requirements for the Degree of
Master of Science in Aeronautical Engineering

Jeffrey L. Wiese, B.S.
Captain, USAF

December 1993

Preface

The purpose of this study was to investigate the effects of using screen mesh, flattened by rolling, for use in screen regenerative heat exchangers. The driving force behind the concept is to reduce the void volume of the regenerator. This reduced void volume should improve the overall performance of a cryocooler. The research was sponsored by Mr. Robert Vacek of the Space Thermal Technologies Branch at Phillips Laboratory in Kirtland Air Force Base NM. The topic was suggested by Dr. Ray Radebaugh at the Chemical Science and Technology Laboratory, National Institute of Standards and Technology, Boulder CO.

In the process of preparing this thesis I had help from many people. In addition, to Mr. Vacek and Dr. Radebaugh I also was blessed with the assistance of Mr. Ron White who shared his years of cryocooler experience with me. Mr. Tim Hancock and Mr. Andy Pitts provided the technical assistance I needed to get the job done. Also, my advisor, Major W. Jerry Bowman, kept me from straying from my objective and was always willing to help. Finally, this paper would have been unreadable without the persistent proofreading of my girlfriend, Ms. Kerrie Lalikos.

Jeffrey L. Wiese

Table of Contents

List of Figures

List of Tables

List of Symbols

a	constant used in curve fit solution for N_{tu}
A	exchanger total heat transfer area
A_c	exchanger minimum free-flow area (pA_{fr})
A_{fr}	exchanger total frontal area
A_s	solid matrix cross-sectional area available for thermal conduction
b	constant used in curve fit solution for N_{tu}
c_p	Specific heat at constant pressure
c_s	matrix material specific heat
C_D	drag coefficient per screen
C_v	flow coefficient for sizing valves
d	wire diameter
D	inside diameter of regenerator
f	friction factor, $\{\rho\tau_o/(G^2/2g_c)\}$
f_o	friction factor for unrolled screen
F	iteration variable used to find Re'
g_c	proportionality factor in Newton's second law
G	exchanger flow-stream mass velocity (W/A_c)
G_{max}	maximum mass velocity in the matrix ($W/\alpha A_{fr}$)
h	convection heat transfer coefficient
j_H	Colburn factor, ($\mathrm{StPr}^{2/3}$)
j_{Ho}	Colburn factor for unrolled screen
k_e	effective thermal conductivity of matrix
k_l	liquid thermal conductivity
k_s	matrix thermal conductivity
K	constant based on geometry for rotameter
L	length of matrix in flow direction
maximum slope	dimensionless slope of temperature vs. time
mesh	mesh size, wires/inch
N_{tu}	number of heat transfer units, hA/Wc_p
p	porosity
p_o	porosity of unrolled screen
P_1	pressure at entrance to the regenerator
P_{baro}	barometric pressure
P_{meter}	gage pressure of the flow entering the meter in Pa
R	fraction roll, ($1-\delta/\delta_o$)
R	gas constant for helium
Re	Reynolds number for internal flow, ($4r_hG/\mu$)
Re'	modified Reynolds based on internal flow
Re_d	Reynolds number for external flow, (dG_{max}/μ)
Re_o	Reynolds number for internal flow for unrolled screen

r_h	hydraulic radius, LA_c/A
$SCFM_{air}$	standard cubic feet per minute of air
St	Stanton number, (h/Gc_p)
T^*	dimensionless temperature, $\{(T_{f2}-T_i)/(T_{f1}-T_i)\}$
$T^*_{measured}$	measured dimensionless temperature
$T^*_{regression}$	dimensionless temperature resulting from linear regression of $T^*_{measured}$
T_1	temperature entering the regenerator in ^oK
T_2	temperature exiting the regenerator in ^oK
T_3	secondary flow temperature in ^oK
T_{f1}	inlet temperature of fluid after time equal zero
T_{f2}	outlet temperature of fluid
T_i	initial temperature of matrix and fluid
$\overline{T}_{f1}$	average inlet temperature after the step change
$\overline{T}_{i1}$	average inlet temperature before the step change
$\overline{T}_{i2}$	average outlet temperature before the outlet temperature began to change.
v_1	specific volume at exchanger entrance
v_2	specific volume at exchanger exit
v_m	mean specific volume, $(v_1 + v_2)/2$
W	mass flow rate
W_{air}	mass flow rate of air at standard conditions
W_{He}	mass flow rate of helium at test conditions
W_s	mass of matrix
x_t	ratio of transverse spacing to wire diameter
y	height of "bob" in tube

Greek symbols

δ	thickness of screen
δ_o	thickness of screen before rolling
θ	time
λ	longitudinal conduction parameter, $\{(k_s A/(Wc_p L)\}$
μ	viscosity
ρ	density (inverse of specific volume v)
ρ_{air}	density of air at standard atmosphere
ρ_b	density of the bob (metal)
ρ_f	density of the flow
ρ_{He}	density of helium at test conditions
ρ_s	density of matrix (304 stainless steel)
σ	ratio of minimum free-flow area to frontal area $\{(x_t - 1)/(x_t)\}^2 = (1 - d\cdot mesh)^2$
τ	time parameter, $hA\theta/(W_s c_c)$
τ_o	unit surface shear stress

Other Variables

Δj_H	uncertainty of j_H
ΔP	pressure drop across matrix
ΔRe	uncertainty of Re
ΔRe_d	uncertainty of Re_d
ΔW	uncertainty of mass flow rate
$\Delta(\Delta P)$	uncertainty of ΔP
$\Delta(\%scale)$	smallest resolution of rotameter
$\Delta\left(\left.\frac{dT^*}{d\theta}\right\|_{max}\right)$	uncertainty of slope of T^*
$\%scale$	scale reading on rotameter

Abstract

This study investigated the effect on heat transfer and friction characteristics for screen regenerative heat exchangers with the screen thickness reduced by rolling. The experiments were performed on 250 and 325 mesh, 304 stainless steel screen using helium gas. Reynolds numbers, based on hydraulic radius, Re, were between 10 and 100. Both the Colburn factor, $St\mathrm{Pr}^{2/3}$, and friction factor, f, decreased as the screen thickness was reduced. A correlation for predicting f was found. The coefficient of drag per screen, C_D, remained nearly unchanged for thicknesses reduced not more than 30 percent. The decrease in Colburn factor was significant for Re less than 40. For $40 < \mathrm{Re} < 100$ the decrease in Colburn factor was less than the experimental uncertainty.

EXPERIMENTAL ANALYSIS OF HEAT TRANSFER CHARACTERISTICS AND PRESSURE DROP THROUGH SCREEN REGENERATIVE HEAT EXCHANGERS

I. Introduction

This research experimentally investigated the effects of using screen mesh, flattened by rolling, for use in regenerative heat exchangers. This chapter explains the reasons for the research and introduces the approach. The background explains the application of regenerative heat exchangers and how rolled screen has potential advantages. In addition, the experimental approach's history is discussed. Finally, the objective is stated and the approach used to reach this objective is explained.

Background

Regenerators and Cryocoolers. Currently, Phillips Laboratory at Kirtland Air Force Base, New Mexico is pursuing using Stirling cycle cryocoolers for space borne use. The typical purpose of space borne cryocoolers is to cool infrared sensors and superconductive electronic devices (Chan, Tward, and Burt 1990:1239). These applications typically require regenerative heat exchangers,

regenerators, (Chan, Tward, and Burt, 1990:1240). One possible choice of matrix material is wire screen.

Walker provided definitions for cryocoolers and regenerators. First, he defined a cryocooler as "... a device or ensemble of equipment for producing refrigeration at temperatures less than 120 K" (Walker, 1983:1). Later he said that regenerators were one of the two typical types of heat exchangers used in cryocoolers. He stated "A regenerative heat exchanger has a single set of flow passages through which the hot and cold fluids flow alternately and periodically" (Walker, 1983:5).

Walker provided a definition of the ideal regenerator which also provided an understanding of a regenerator's function.

> The ideal regenerator can be conceived as a thermodynamic "black box" accepting gas at temperature T_c and heating it to T_h. After some time the flow is reversed and gas enters at T_h leaving T_c (sic). The pressure drop across the regenerator would be zero. When used in Stirling engines where dead space is an important parameter, the ideal regenerator has zero void volume. (Walker, 1983:36)

According to Walker's definition, dead space refers to the volume filled by the working fluid which is not in the compression or expansion space of the cryocooler (Walker, 1983:577). T_c and T_h represent the cold and hot temperatures, respectively.

Walker also discussed regenerator design for Stirling coolers as follows:

> for maximum heat capacity -- a large, solid matrix,
> for minimum flow losses -- a small, highly porous matrix,
> for minimum dead space -- a small, dense matrix,
> for maximum heat transfer -- a large, finely divided matrix,
> for minimum contamination -- a matrix with no obstruction. (Walker, 1983:44)

Walker's third point, minimum dead space, is the driving interest behind this investigation. The correlation to dead space holds also for non-ideal cycles. Tailor and Narayankhedkar (1990:1411) performed a numerical analysis which allowed for imperfect regeneration in a piston-displacer Stirling cryocooler. Their graphs illustrated that the refrigerating capacity decreased as the dead volume increased even for non-ideal regenerators. In addition, Atrey, Bapat, and Narayankhedkar (1991:1049) performed a numerical analysis on Stirling cycle wire mesh regenerators. In their analysis of mesh size (wires per inch of screen) they varied the wire diameter which changed the dead volume within the regenerator. They observed "... the maximum effectiveness is obtained at the minimum dead volume combination for a given mesh size." (Atrey, Bapat, and Narayankhedkar 1991:1049)

As the last three references stated, decreasing the dead space within a regenerator is an important concept. An extension to Atrey, Bapat and Narayankhedkar's (1991) observation implies that methods to decrease the dead space for a particular mesh size are worth considering. One

possible method to accomplish this is to flatten the screens before assembling the regenerator.

Gary and Radebaugh (1991) completed an improved numerical model for calculating regenerator performance, "Regen 3.1." The model incorporated six different matrix geometries. Wire screen was one of the geometries incorporated. Radebaugh stated in telephone conversations with the investigator (1993) that he would like to incorporate rolled screen into his analysis. He had already supervised some tests with 200 mesh screen that had not been fully analyzed. In fact, he recommended the topic of investing flattened screens for other mesh sizes to provide breadth to the data base.

Thus, to approach the zero dead volume of the ideal Stirling cycle regenerator, rolling the screen used for a regenerator matrix provides possible advantages. However, pressure losses could prove to be a problem. Since only limited experimentation with rolled screen regenerators has been performed more data are needed to gain an understanding of its effect. Once this is done, the feasibility of rolled screen in cryocooler regenerators will be known.

Previous Experimental Research. The research method used in this investigation is based on three references. The first two references were test results for woven screen. The third reference used unrelated matrixes, but provided the technique to evaluate heat transfer.

The two references for previous research on woven screen were Kays and London (1984) and Tong and London (1957). Kays and London (1984) compiled several series of tests that were performed in the late 1940's and 1950's. The tests related to compact heat exchangers. One of the matrixes tested was crossed rod or woven screen. Tong and London (1957), however, were the actual source for the data in Kays and London (1984). Tong and London presented results for hydraulic Reynolds numbers between 5 and 100,000. These two references provided the comparison data for this research. However, the tests were performed under different conditions. The working fluid was air and the geometries were much larger. These two references also provided the necessary theory to perform the friction calculations for this research.

Pucci, Howard, and Piersal (1967) detailed the history and application of the single-blow transient testing technique. The matrixes they tested were not similar to screen matrixes. However they explained how to apply the single-blow transient testing technique to test compact heat exchangers. A primary advantage to the single-blow transient testing technique is its minimal equipment requirements.

Literature searches were completed to find research performed on rolled screen. No references were found. The searches were done on the following three data bases:

Defense Technical Information Center (DTIC), National Aeronautics and Space Administration (NASA), and DIALOG Information Retrieval Service.

Objective

The objective of this research was to experimentally determine the advantages and disadvantages of using screen mesh flattened by rolling in regenerative heat exchangers. There were two aspects investigated. The first aspect was the heat transfer properties, quantified in terms of number of heat transfer units, N_{tu}, and converted to the Colburn factor, j_h. The heat transfer properties were expected to improve by rolling the screens. The second aspect was friction losses. The friction loses were expected to increase with rolling the screen and were quantified in terms of the friction factor, f. The opposing effects of heat transfer and friction losses provided the point of interest of this research.

Approach

The primary approach to this research was to build a test apparatus that could provide a step temperature change by quickly changing the inlet flow with the use of a four-way valve. In addition, the system measured inlet pressure, pressure drop, mass flow rate, and transient temperature response. The pressure and flow rate information provided the data necessary to calculate the friction, f, from

equations in Tong and London (1957) and Kays and London (1984). The transient temperature response was used to calculate the heat transfer information using the single-blow transient testing technique (Pucci, Howard and Piersall, 1967).

Test Parameters. The test parameters were as follows:

1. Screen mesh material: 304 stainless steel
2. Screen mesh size: 250 and 325 mesh
3. Fraction roll: 0, 0.15, 0.30, 0.50
4. Regenerator tubing (case) 304 stainless steel
5. Regenerator dimensions: 15.0 mm inside diameter
   15.9 mm outside diameter
   38 mm long
6. Working fluid: Helium gas
7. Inlet pressures (P_1): 10, 20 and 30 atm
8. Reynolds number (based on hydraulic radius): roughly 10, 20, 40, and 100
9. Initial temperature: 292 - 297 K
10. Final temperature (after step change): 285 - 300 K

II. Theory and Experimental Analysis

This chapter provides a brief explanation of the theory upon which the experimental techniques to measure friction and heat transfer were based. Then the investigator's application of this theory is explained. In addition, the empirical results from previous research are presented. Finally, the method of performing the uncertainty analysis is explained. Since a central source of information for compact heat exchangers is Compact Heat Exchangers, (Kays and London, 1984) its format and choice of variables were followed as much as possible. In the case of the transient temperature response some variables were used from "The Single-Blow Transient Testing Technique for Compact Heat Exchangers Surfaces," (Pucci, Howard and Piersall, 1967).

Friction

Friction was analyzed using two different dimensionless quantities. These two quantities were the friction factor, f, and the drag coefficent, C_D. The next few paragraphs describe both quantities and develop the equations used to calculate f and C_D. Then the empirical curve fit from prior research is stated.

Friction factor definition. Friction was one of the two major properties to measure. Kays and London (1984) defined the mean friction factor (similar to Fanning

friction factor for flow through tubes) for a matrix surface as $f \equiv \frac{\rho \tau_0}{G^2/2g_c}$. They applied conservation of momentum for a heat exchanger with uniform frontal and exit areas to obtain the following equation.

$$\frac{\Delta P}{P_1} = \frac{G^2}{2g_c}\frac{v_1}{P_1}\left[\left(1+p^2\right)\left(\frac{v_2}{v_1}-1\right)+f\frac{A}{A_c}\frac{v_m}{v_1}\right] \qquad (2.1)$$

where

ρ = density (inverse of specific volume v)
τ_o = unit surface shear stress
G = exchanger flow-stream mass velocity (W/A_c)
g_c = proportionality factor in Newton's second law
W = mass flow rate
ΔP = pressure drop across matrix
P_1 = pressure at entrance to the heat exchanger
v_1 = specific volume at exchanger entrance
v_2 = specific volume at exchanger exit
v_m = mean specific volume
p = porosity of matrix surface
A = exchanger total heat transfer area
A_c = exchanger minimum free-flow area (pA_{fr})
A_{fr} = exchanger total frontal area

Note: The first term inside the square brackets is flow acceleration and the second term is the core friction.

Friction Operating Equation. The investigator solved Eq. 2.1 for the friction factor,

$$f = \frac{v_1}{v_m}\frac{A_c}{A}\left[2\frac{\Delta P g_c}{G^2 v_1}-\left(1+p^2\right)\left(\frac{v_2}{v_1}-1\right)\right]. \qquad (2.2)$$

The next step was to apply simplifying assumptions to make this equation a function of the various measured parameters. The first assumption was that the gas was thermally perfect. Next, the mean specific volume was

approximated as $v_m = (v_1 + v_2)/2$. This approximation for v_m was recommended by Kays and London (1984). (The specific method used to calculate the screen properties (A, A_c, p, and r_h) and mass flow rate, W, are explained in later sections of this chapter). In addition, frontal area, A_{fr}, was assumed circular. The measurements were made in metric units so $g_c = 1$. In addition, the effects of Mach number were assumed negligible since the Mach numbers were less than 0.1. The testing was near ambient temperature and the regenerator case was insulated. Thus, the process was assumed adiabatic for the friction measurement experiments. These last assumptions allowed the static and stagnation temperatures to be the same and $T_1 \approx T_2$. Thus, the final operating equation for the friction factor was

$$f = \frac{2}{1+\frac{P_1}{P_1-\Delta P}}\left(\frac{A_c}{A}\right)\left[\frac{\Delta P P_1}{8RT_1}\left(\frac{p\pi}{W}\right)^2 D^4 - \left(1+p^2\right)\left(\frac{P_1}{P_1-\Delta P}-1\right)\right]. \qquad (2.3)$$

D was the inside diameter of the regenerator tube and R was the gas constant for helium.

Previous Results. Kays and London (1984) provided a graph of f vs. Re for an infinite randomly stacked woven-screen matrix. This graph was an excerpt from Tong and London (1957). Tong and London provided curves of f vs. Re for lines of constant porosity. In addition, they presented graphs of C_D vs. Re_d that were the basis of their empirical curve fit.

$$\log_{10} C_D = \frac{1.33}{p^2} \mathrm{Re}_d^{-0.33} - \frac{0.54}{p} \qquad (2.4)$$

where

C_D = drag coefficient per screen
Re = Reynolds number for tube like flow or internal flow
Re_d = Reynolds number for flow over a body or external flow

Note: Both Reynolds numbers, Re and Re_d, are explained in further detail in a later section in this chapter.

Tong and London derived the following conversion relationship for "essentially constant-density flow" (Tong and London, 1957:1561):

$$\frac{f}{C_D} = \left(\frac{r_h}{\delta}\right)\left(\frac{p}{\sigma}\right)^2. \qquad (2.5)$$

where

δ = screen thickness
r_h = hydraulic radius, LA_c/A
L = Length of matrix in flow direction (tube length - gap (explained in Chapter III))
σ = ratio of minimum free-flow area to frontal area
$\sigma = (1 - d \cdot mesh)^2$
d = wire diameter
$mesh$ = mesh size, wires/inch

Equation 2.5 proved very useful when converting test data for f to C_D which allowed another perspective as well as a comparison to the results of Tong and London.

Heat Transfer

Common practice calls for the heat transfer results to be in the form $\mathrm{StPr}^{2/3}$. This term will be commonly referred to in its shorter form as the Colburn factor, $j_H = \mathrm{St}\,\mathrm{Pr}^{2/3}$.

First, the method detailed by Pucci, Howard and Piersall (1967) to find the dimensionless quantity number of heat transfer units, N_{tu}, is explained. Next this section explains the transition of N_{tu} to j_H. Finally, the investigator's application of the entire process is detailed.

Single-Blow Transient Testing Technique. The single blow transient testing technique used in the investigation was based on the writing of Pucci, Howard and Piersall (1967). They summarized the historical development of the technique by other researchers. They also added their own modification. The following is a direct quotation from their paper explaining the final result:

> .... The analysis is based upon an energy balance on an element of the porous solid ...
>
> Assumptions made in the analysis are:
> (a) Properties of the fluid are temperature independent
> (b) Fluid flow is steady
> (c) Porous solid is homogeneous
> (d) Thermal conductivity of both fluid and solid is infinite perpendicular to the fluid flow direction
> (e) Thermal conductivity of fluid is zero in the flow direction.
>
> Initial boundary conditions are:
> (a) The matrix is initially at a uniform temperature
> (b) At time equal to zero, the temperature of the entering fluid changes instantaneously to a different, constant value, i.e., a step change in fluid temperature
> (c) The matrix boundaries are adiabatic
> (Pucci, Howard and Piersall, 1967:29)

One additional assumption was that the thermal capacity of the gas (mass x specific heat) contained in the matrix was much less than the thermal capacity of the solid.

Thermal conduction in the solid, parallel to the direction of the flow was represented by the dimensionless longitudinal conduction parameter defined as $\lambda = \frac{k_s A_s}{W c_p L}$.

where

k_s = matrix thermal conductivity
A_s = solid matrix cross-sectional area available for thermal conduction
L = length of matrix
c_p = specific heat at constant pressure

Approximation of Zero Longitudinal Conduction. Since λ was an important factor in the procedure, an estimate of λ was required before proceeding with further calculations. A simple and straight forward approximation of thermal conductivity perpendicular to the screens for liquid saturated wrapped screen is (Chi, 1976:50)

$$k_e = \frac{k_l\left[(k_l + k_s) - (1-p)(k_l - k_s)\right]}{\left[(k_l + k_s) + (1-p)(k_l - k_s)\right]}. \qquad (2.6)$$

where

k_e = effective thermal conductivity
k_l = liquid thermal conductivity
p = porosity

The approximation for λ resulted by substituting the thermal conductivity of helium for k_l and realizing that

$k_e A_{fr} \approx k_s A_s$. For constant length and frontal area the maximum value for λ_{max} occurred with minimum mass flow and maximum k_e (minimum porosity). As shown in Appendix C, p_{min} = 0.4245 which yielded k_e = 0.524 W/mK. In addition, the frontal area was 0.176 x 10^{-3} m^2, the length was 0.0371 m (Appendix C), and the minimum flow rate was approximately 0.28 x 10^{-3} kg/s (Appendix D). Thus, $\lambda_{max} \approx 0.0017$. Pucci, Howard and Piersall (1967:30) tabulated finite difference results that included λ but the minimum non-zero value was 0.005 which is greater than the estimated value for λ_{max}. Therefore, the investigator used the approximation of zero thermal conductivity in the direction of the flow.

The approximation $\lambda \approx 0$ allowed the use of the exact solution below.

$$slope = \frac{d\left[\frac{T_{f2} - T_i}{T_{f1} - T_i}\right]}{d\left[\frac{\tau}{N_{tu}}\right]} = \frac{N_{tu}^{\ 2}}{\sqrt{N_{tu}\tau}}\left[-iJ_1\left(2i\sqrt{N_{tu}\tau}\right)\right]e^{-(N_{tu}+\tau)} \qquad (2.7)$$

where

T_i = initial temperature of matrix and fluid
T_{f1} = inlet temperature of fluid after time equal zero
T_{f2} = outlet temperature of fluid
τ = time parameter, $hA\theta/(W_s c_c)$
N_{tu} = number of heat transfer units, $hA/(Wc_p)$
h = convection heat transfer coefficient
W_s = mass of matrix
c_s = matrix material specific heat
θ = time
$-iJ_1(ix)$ = modified (Hyperbolic) Bessel Function

Equation 2.7 predicts slope of the dimensionless temperature as a function of N_{tu} and time. From the equation the *slope* can be found for any time.

As explained in Pucci Howard and Piersall (1967); for a given N_{tu} the *maximum slope* (using Eq. 2.7) has a unique value. Thus, if the *maximum slope* can be measured experimentally the N_{tu} can be found.

The *maximum slope* for a given N_{tu} was found by gradually increasing the time parameter, τ. The *slope* steadily increased until the maximum value was reached. Once the *slope* began to decrease, the *maximum slope* for the given N_{tu} was known. Pucci, Howard and Piersall performed this proceedure for N_{tu} up to 60. This was insufficient, so the investigator extended the curve. The resulting N_{tu} vs. *maximum slope* is graphically illustrated in Fig. 2.1 and tabulated in Appendix B.

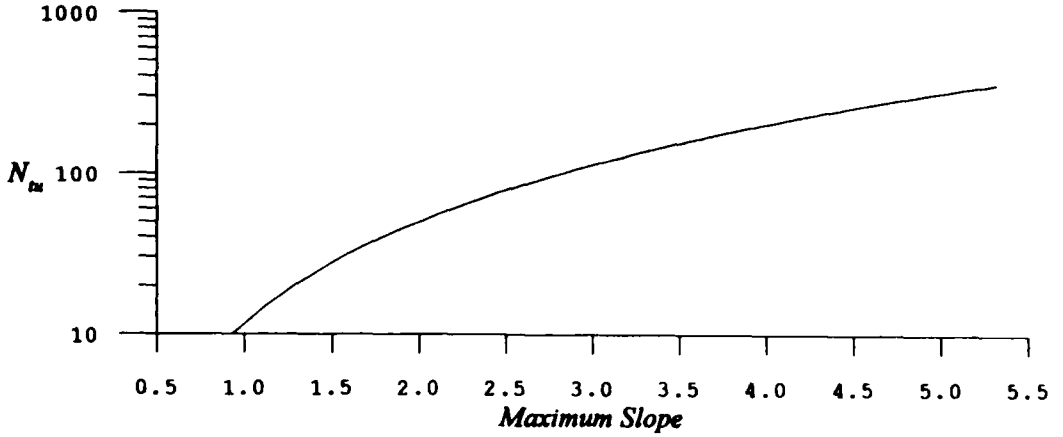

Figure 2.1. Number of Transfer Units vs. Maximum Slope

Application of Single Blow Technique. The investigator defined

$$T^* = \left[\frac{T_{f2} - T_i}{T_{f1} - T_i}\right]. \tag{2.8}$$

In addition, the dimensional values which defined N_{tu} and τ were substituted into the left hand side of Eq. 2.7 to obtain

$$maximum\ slope = \frac{d\left[\frac{T_{f2} - T_i}{T_{f1} - T_i}\right]}{d\left[\frac{\tau}{N_{tu}}\right]} = \frac{W_s c_s}{W c_p}\left.\frac{dT^*}{d\theta}\right|_{max}. \tag{2.9}$$

For each test, the maximum slope defined by Eq. 2.9 was found from the experimental values of temperature, time, screen mass, mass flow rate and tabulated specific heats. Knowing the *maximum slope*, the N_{tu} could be determined from the N_{tu} vs. *maximum slope* graph in Fig 2.1 or the table in Appendix B. The next step was to consider the definition of Stanton number, $St = \frac{h}{Gc_p}$. From the definitions of G (Eq. 2.1) and Stanton number, St, the desired Colburn factor, j_H, can be related to N_{tu}.

$$j_H = St\,\mathrm{Pr}^{2/3} = N_{tu}\left(\frac{A_c}{A}\right)\mathrm{Pr}^{2/3}. \tag{2.10}$$

Method to Find *Maximum Slope*. The method the investigator used to find *maximum slope* relied heavily upon the spreadsheet

Quattro Pro SE. As described in Chapter III, the transient temperature response was recorded to data files. For each test the investigator would read the data files into a base spreadsheet that was already configured for the analysis. The goal was to find $\left.\frac{dT^*}{d\theta}\right|_{max}$ as required from Eq. 2.9. To achieve this goal, the investigator made a slight modification to the equation for T^* due to the slight difference (less than 0.3 K) that sometimes existed between measured values for T_1 and T_2 at steady-state before the step temperature change. The following approximation was used

$$T^* = \frac{\left[T_{f2} - T_i\right]}{\left[T_{f1} - T_i\right]} \approx \frac{\left[T_{f2} - \overline{T}_{i2}\right]}{\left[\overline{T}_{f1} - \overline{T}_{i1}\right]}. \qquad (2.11)$$

where

$\overline{T}_{f1}$ = average inlet temperature after the step change
$\overline{T}_{i1}$ = average inlet temperature before the step change
$\overline{T}_{i2}$ = average outlet temperature before the outlet temperature began to change.

A quick summary using Fig. 2.2 is useful. The two curves T_1 and T_2 represent the measured temperatures at the inlet and outlet, respectively, of the regenerator. The horizontal distances shown with $\overline{T}_{f1}$, $\overline{T}_{i1}$, and $\overline{T}_{i2}$ illustrate the time interval for which the average values were calculated. Equation 2.11 was applied to $\overline{T}_{f1}$, $\overline{T}_{i1}$, and $\overline{T}_{i2}$ to calculate $T^*_{measured}$. Finally, the heavy line labeled $T^*_{regression}$ (scale is on right hand side of graph) was the result of a linear regression performed on $T^*_{measured}$ for the time interval

shown. The slope of $T^*_{regression}$ was the measured value for $\left.\frac{dT^*}{d\theta}\right|_{max}$.

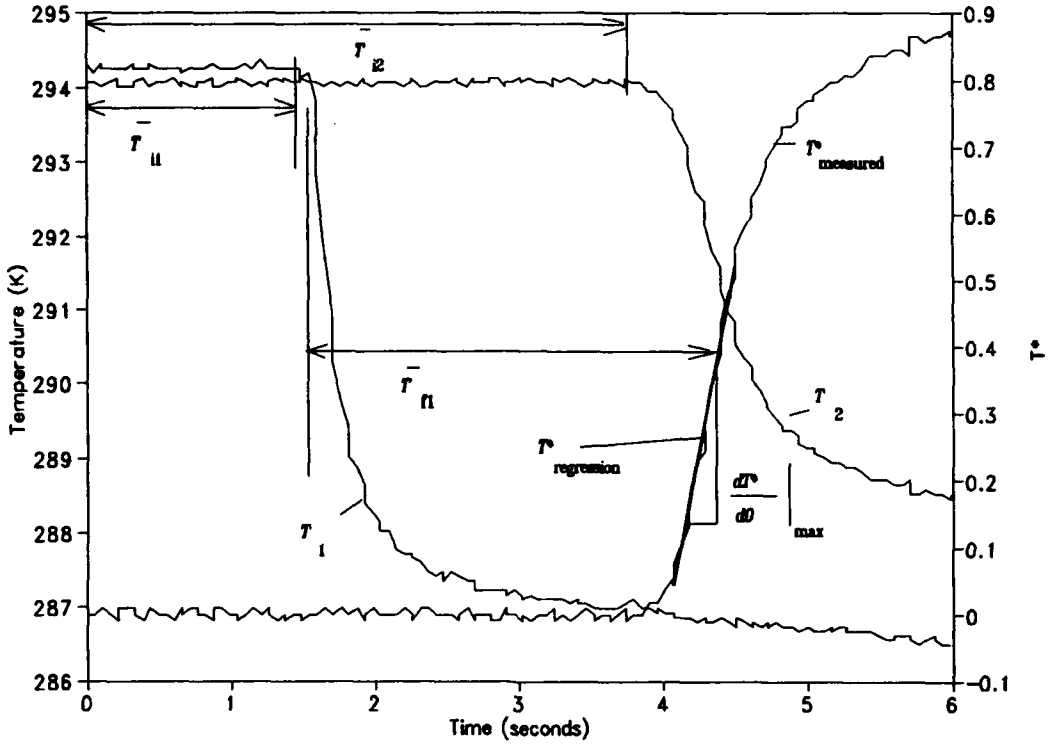

Figure 2.2. Sample Quattro Pro Analysis of $\left.\frac{dT^*}{d\theta}\right|_{max}$ Showing $\bar{T}_{f1}$, $\bar{T}_{i1}$, and $\bar{T}_{i2}$

Before proceeding, an explanation $\bar{T}_{f1}$ is necessary. Since the actual inlet temperature was not a true step function, the investigator made an approximation. The approximation was based on an average temperature. $\bar{T}_{f1}$ was the average of T_1 over the time interval beginning when T_1

had changed roughly 1 K and ending at the time of $\left.\frac{dT^*}{d\theta}\right|_{max}$ (maximum slope of T_2).

Once the values for $\bar{T}_{f1}$, $\bar{T}_{i1}$, and $\bar{T}_{i2}$ were found the process of finding the slope began. First, these values were substituted into Eq. 2.11 to plot T^*. From the plot of T^* vs. time, a time interval was visually selected to perform a linear regression of T^* vs. time. Then the linear regression result was plotted with T^* to ensure a satisfactory regression had been selected. If the regression appeared to be unsatisfactory the time interval was altered appropriately and its plot inspected. This process was continued (using the same $\bar{T}_{f1}$, $\bar{T}_{i1}$, and $\bar{T}_{i2}$) until the linear regression accurately represented $\left.\frac{dT^*}{d\theta}\right|_{max}$.

Finally, the *maximum slope* was calculated using Eq. 2.9. Then the investigator used the curve fit from Appendix B to calculate N_{tu}.

$$N_{tu} = a(\text{maximum slope})^b \qquad (2.12)$$

maximum slope	*a*	*b*
[0.92, 2.00)	11.77	2.084
[2.00, 2.80)	12.19	2.023
[2.80, 5.32)	12.38	2.008

Equation 2.12 allowed automation of the data analysis in the same spreadsheet used to calculate the friction results.

Finally, the Colburn factor, j_H, was calculated using Eq. 2.10.

Previous Results. Pucci, Howard, and Piersall (1967) performed their tests on matrixes other than woven screen. However, Kays and London (1984) provided a graph of $StPr^{2/3}$ vs. Re for infinite randomly stacked woven-screen matrix. This graph was an excerpt from Tong and London (1957). Tong and London provided curves of $StPr^{2/3}$ vs. Re for lines of constant porosity. In addition, they provided an empirical curve fit for screen or crossed rod matrixes and $0.55 < p < 0.85$.

$$j_H = StPr^{2/3} = 0.375 Re^{-0.375} \qquad (2.13)$$

The two equations below were iterated to calculate the modified Reynolds number, Re'. The first iteration started by letting Re' = Re. Then the first iteration for F was found and the second iteration for Re' was calculated. The solution converges after several iterations.

$$F = 1.155 - 0.0601(\log_{10} Re'), \quad Re' = \frac{1-Fp}{Fp} Re \text{ for } Re' < 1800$$

Screen Properties

This section details the assumptions and equations used to calculate the screen properties (A, p, A_c, r_h, and R).

Matrix Total Area, A. The primary assumption by the investigator was that the area, A, was approximately equal to the area of a long thin wire with diameter d and mass W_s. In addition, effects of the regenerator case, or tube, were assumed negligible, since the tube's surface area was small

compared to the surface area of all the screen it contained. Thus, the resulting equation was

$$A = \frac{4W_s}{d\rho_s}. \tag{2.14}$$

where

W_s = measured mass of the screen in the regenerator
d = wire diameter as published by the manufacturer
ρ_s = density of solid 304 stainless steel (Appendix A)

Porosity. The porosity, p, of the matrix was calculated using masses. The investigator derived Eq. 2.15. He assumed the matrix to be homogeneous and used the ratio of the measured mass to the mass of a solid cylinder.

$$p = 1 - \frac{4W_s}{\pi D^2 \rho_s L} \tag{2.15}$$

Exchanger Minimum Free Flow Area. The exchanger minimum free flow area, A_c, was derived from an equation in Kays and London (1984:44),

$$A_c = pA_{fr} = \frac{1}{4} p\pi D^2 \tag{2.16}$$

Hydraulic Radius. The hydraulic radius, r_h, was calculated from another relationship from Kays and London (1984:44).

$$r_h = \frac{A_c}{A} L \tag{2.17}$$

Fraction Roll. The investigator derived a relationship to calculate the fraction roll, R.

$$R = 1 - \frac{\delta}{\delta_o} \tag{2.18}$$

where

δ = measured thickness of screen
δ_o = measured thickness of screen before rolling

Mass Flow Rate

As will be discussed in Chapter III, the instrument used to measure mass flow rate was a rotameter calibrated for standard cubic feet per minute (*SCFM*) of air. Since the rotameter was calibrated for air the investigator needed a method to convert the readings to helium. Dally, Riley and McConnel (1984) provided a description of the theory of rotameters. A rotameter is a tapered tube with a "bob" which is suspended in the flow of the fluid to be measured. Because of the shape of the "bob", the effect of viscosity was negligible. Dally, Riley and McConnel (1984) derived the following linear relationship, because of the geometry of the tube and bob.

$$W = K\sqrt{(\rho_b - \rho_f)\rho_f y} \qquad (2.19)$$

where

W = mass flow rate of the flow
K = constant based on geometry
ρ_b = density of the bob (metal)
ρ_f = density of the flow
y = height of "bob" in tube

The investigator used Eq. 2.19 to derive the conversion to mass flow rate of helium. Since ρ_{air} and ρ_{helium} are both much less than ρ_b, the ratio of flow rates for two flows

with identical rotameters with the bob in the same position is

$$\frac{W_{He}}{W_{air}} = \sqrt{\frac{\rho_{He}}{\rho_{air}}} \; . \qquad (2.20)$$

where

W_{He} = mass flow rate of helium at test conditions
ρ_{He} = density of helium at test conditions
W_{air} = mass flow rate of air at standard conditions
ρ_{air} = density of air at standard atmosphere

The mass flow rate of the air can be found from:

$$W_{air} = SCFM_{air}\rho_{air} \qquad (2.21)$$

The calibration plate on the rotameter stated that $SCFM_{air}$ = 0.1345 x percentage scale of the meter. Furthermore, the plate defined a standard atmosphere as 70 ^{o}F and 1 atm. Using this relation and assuming thermally perfect gases the investigator derived the equation to calculate helium mass flow rate from the rotameter reading.

$$W = W_{He} = 1.526 \times 10^{-6} \sqrt{\frac{P_{baro} + P_{meter}}{T_1}} \times (\%scale) \;\; \text{kg/s} \qquad (2.22)$$

where

P_{baro} = barometric pressure in Pa
P_{meter} = gage pressure of the flow entering the meter in Pa
T_1 = temperature entering the regenerator in ^{o}K

The temperature was assumed to remain constant since all tubing essentially remained at room temperature. This was acceptable because all flow rates were measured before the step temperature change was initiated.

Reynolds Number

There were two types of Reynolds number used in this investigation. The internal flow Reynolds number, Re, was used to present data in the standard format used in Kays and London (1984). At times however, a Reynolds number based on external flow, Re_d, was found to be useful in the discussion in Chapter IV.

The first Reynolds number was for internal flow. Kays and London (1984) presented the definition

$$\mathrm{Re} = \frac{4 r_h G}{\mu}. \qquad (2.23)$$

where

G = flow stream mass velocity ($\frac{W}{A_c}$ or $\frac{W}{pA_{fr}}$)

r_h = hydraulic radius ($\frac{A_c}{A} L$)

μ = viscosity

The viscosity is listed in Appendix A and was based on the regenerator inlet temperature T_1.

The second type of Reynolds number was for external flow. Tong and London (1957) presented the definition

$$\mathrm{Re}_d = \frac{d G_{max}}{\mu}. \qquad (2.24)$$

where

d = wire diameter
G_{max} = maximum mass velocity in the matrix ($W/\sigma A_{fr}$)
σ = ratio of minimum free-flow area to frontal area
$\sigma = \{(x_t - 1)/(x_t)\}^2 = (1 - d \cdot mesh)^2$
x_t = ratio of transverse spacing to wire diameter

Uncertainty Analysis

An uncertainty analysis was performed on mass flow rate, Reynolds number(s), friction, and heat transfer. Different approaches were used for each parameter, as applicable.

Mass Flow Rate. As explained earlier in this chapter, the mass flow rate was calculated using Eq. 2.20. The form of the equation was $W = C\sqrt{\frac{P_{baro} + P_{meter}}{T_1}} \times (\%scale)$, where C was a constant. The investigator found that P_{baro}, P_{meter}, and T_1 were accurate compared to *%scale*. Due to the limited resolution of the scale on the rotameter, the investigator assumed the resolution to which the scale could be read was 0.5 *%scale* (i.e. $\Delta(\%scale)$ = 0.5 %). So, the method of uncertainty analysis presented by Beckwith, Buck, and Marangoni (1982:269) was applied with *%scale* as the only variable. The uncertainty of mass flow, W, is ΔW.

$$\frac{\Delta W}{W} = \sqrt{\left(\frac{\Delta(\%scale)}{W}\frac{\partial W}{\partial(\%scale)}\right)^2} = \frac{\Delta(\%scale)}{\%scale} \qquad (2.25)$$

Reynolds Number. The two Reynolds numbers were defined in Eqs. 2.23 and 2.24. The properties of the matrix (A, A_c, A_{fr}, L, σ, and p) appeared to be accurate in comparison to the resolution of the rotameter. So, using the same approach as shown for mass flow rate the uncertainty of Re and Re_d was

$$\frac{\Delta \mathrm{Re}}{\mathrm{Re}} = \frac{\Delta \mathrm{Re}_d}{\mathrm{Re}_d} = \frac{\Delta(\%scale)}{\%scale}. \qquad (2.26)$$

Friction. As shown earlier in this chapter, the friction factor, f, was calculated using Eq. 2.3. The two variables that were of most concern were the differential pressure, ΔP and the mass flow rate, W. The uncertainty was found by using a spreadsheet to vary ΔP by its uncertainty, $\Delta(\Delta P)$, and vary W by ΔW. The experience gained while calibrating the differential pressure transducer provided the reference for its accuracy. To find the uncertainty in f, the voltage used for calculating ΔP was varied by ±0.0005 volts and the rotameter reading was varied by ±0.5 *%scale*. The conclusion was that the uncertainty in f ranged from 12 percent at the lowest Re and decreased to 1.1 percent at the highest Re.

Heat Transfer. The heat transfer uncertainty was calculated using the method of Beckwith, Buck, and Marangoni (1982). A rigorous solution would involve partial derivatives of modified Bessel functions. Instead the curve fit derived earlier was employed since it is accurate in the region of interest.

As explained earlier, the heat transfer was calculated using Eq. 2.10 ($j_H = St\,\mathrm{Pr}^{2/3} = N_{tu}\left(\frac{A_c}{A}\right)\mathrm{Pr}^{2/3}$). Again, assuming the matrix properties were accurate and applying the curve fit

$N_{Nu} = a(max\ slope)^b$ to Eq. 2.9, the resulting equation was found to represent the uncertainty in j_H.

$$\frac{\Delta j_H}{j_H} = b\sqrt{\left(\frac{\Delta\left(\left.\frac{dT^*}{d\theta}\right|_{max}\right)}{\left.\frac{dT^*}{d\theta}\right|_{max}}\right)^2 + \left(\frac{\Delta W}{W}\right)^2} \qquad (2.27)$$

The next step was to approximate $\Delta\left(\left.\frac{dT^*}{d\theta}\right|_{max}\right)$. This was accomplished by utilizing the statistical output which Quattro Pro SE generated with the linear regression used to calculate $\left.\frac{dT^*}{d\theta}\right|_{max}$. The percentage error of the slope was calculated by dividing the "standard error of the x-coefficient" by the "x-coefficient" (Borland 1991:479). However, performing the ratio for each test was not as revealing as evaluating this ratio for a random sample and finding the upper bounds of the percentage error. In addition, the investigator observed that the percentage error was dependent on the mass flow rate of the helium. As a result, the percentage error was calculated for a random sample of five tests for each of the four different mass flow rates used in the experimental tests. The result was that the bounds were as follows:

W (10^{-3} kg/s)	0.28	0.56	1.2	2.9
bound(%error)	4	8	13	25

A linear regression of the bounds resulted in the equation

$$\frac{\Delta\left(\left.\frac{dT^*}{d\theta}\right|_{max}\right)}{\left.\frac{dT^*}{d\theta}\right|_{max}} = 7{,}700W + 3.07\%. \qquad (2.28)$$

Thus, the final equation for estimating the Colburn factor was

$$\frac{\Delta j_H}{j_H} = b\sqrt{(77W + 0.0307)^2 + \left(\frac{\Delta W}{W}\right)^2}. \qquad (2.29)$$

III. Experimental Design

In this chapter the equipment used for the experiment is described. First, the overall test apparatus is explained and illustrated. Then, part-by-part each component of the apparatus is explained. This will help to explain the reasons behind any decisions and provide a detailed description of each component and method of use. The effect of components on the data and results is discussed in Chapter IV.

Overall Design

As explained in Chapter II an apparatus was required that provided pressure and temperature sampling before and after the flow entered the regenerator. In addition, it needed to produce a step temperature input. Figure 3.1 is a schematic of the entire apparatus, and Fig. 3.2 is a photograph of the entire apparatus.

Working from left to right across Fig. 3.1 the first item is the two helium tanks which provided the helium for the system. Then, a pressure regulator controlled the pressure of the system. After the pressure regulator the flow was split to provide a cold and warm flow path. The warm flow was room temperature and the cold flow was chilled with an ice bath. Both flows nearly crossed paths at the four-way valve which was quickly switched when the step

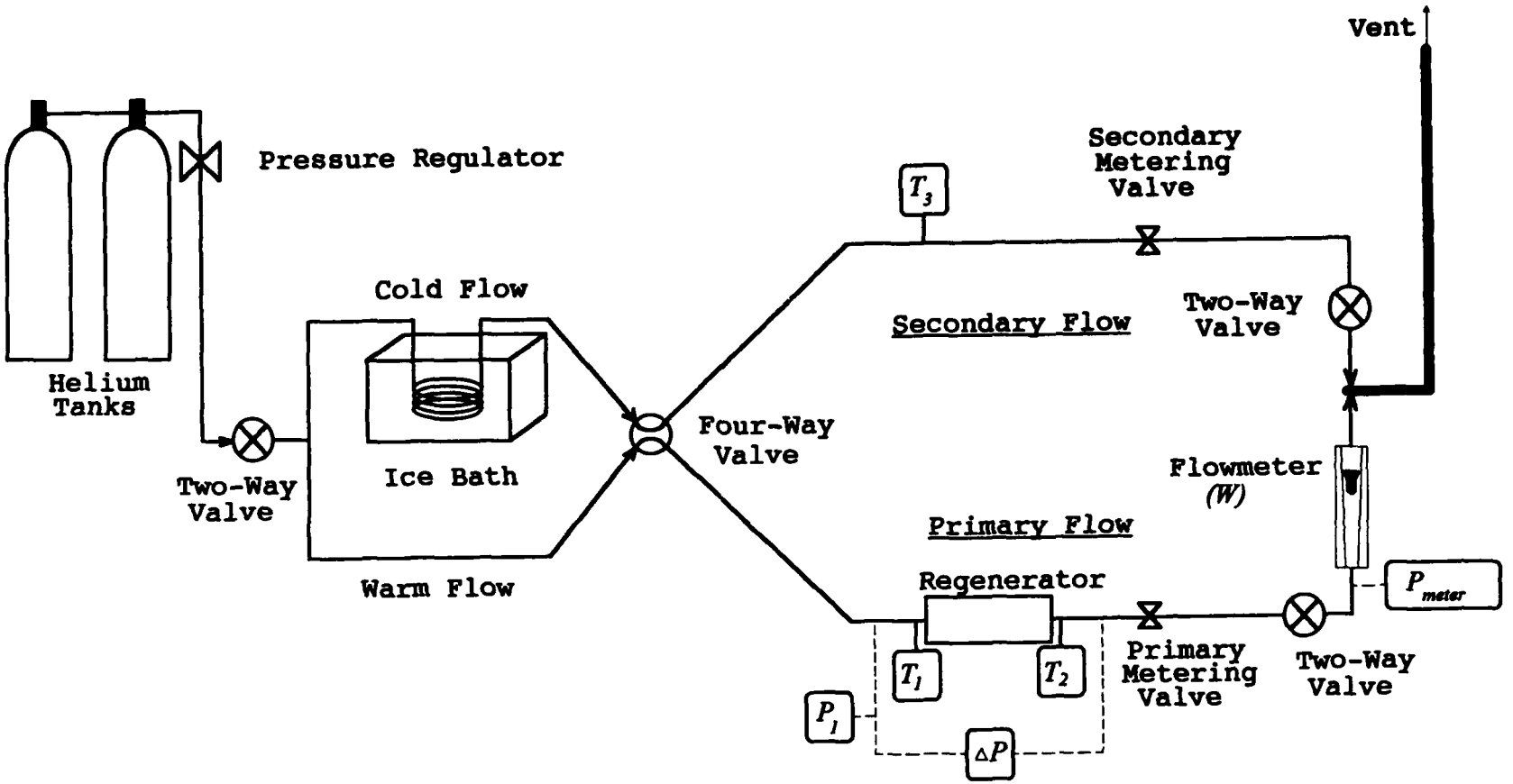

Figure 3.1. Test Apparatus Schematic

temperature change was required (shown in the initial position). Then the flows split into the primary and secondary flows. The primary flow actually flowed through the regenerator for the tests. The inlet and exit temperatures, T_1 and T_2, were measured as well as the inlet pressure, P_1, and the pressure drop, ΔP. The primary metering valve provided precise mass flow control through the regenerator. Finally, the flow meter measured the flow rate through the regenerator. The secondary flow allowed the cold flow to chill the lines leading to the four-way valve. The temperature leaving the four-way valve was measured through the secondary flow line. A metering valve controlled the flow rate through the secondary flow tubing (kept to a minimum). The two flows recombined in the vent line which vented to an exhaust fan.

Regenerator

The regenerator design was based on a design used by Rawlins (1992) at the Chemical Science and Technology Laboratory, National Institute of Standards and Technology (NIST). These tests were performed with the guidance of Radebaugh who recommended investigating rolled screen as mentioned in Chapter I. The NIST regenerator tube was made of stainless steel with a 15.875 mm (5/8 inch) outside diameter, a 0.254 mm (0.010 inch) wall thickness and a length of 122 mm (8.80 inch). Figure 3.3 shows the design

for this thesis. The regenerator was the same outside diameter but the length was significantly less than the NIST regenerator. The shorter length reduced the quantity of screen and labor required. In addition, the lower pressure drop, ΔP, could be measured by pressure transducers "on-hand" at the AFIT Department of Aeronautics and Astronautics Laboratories.

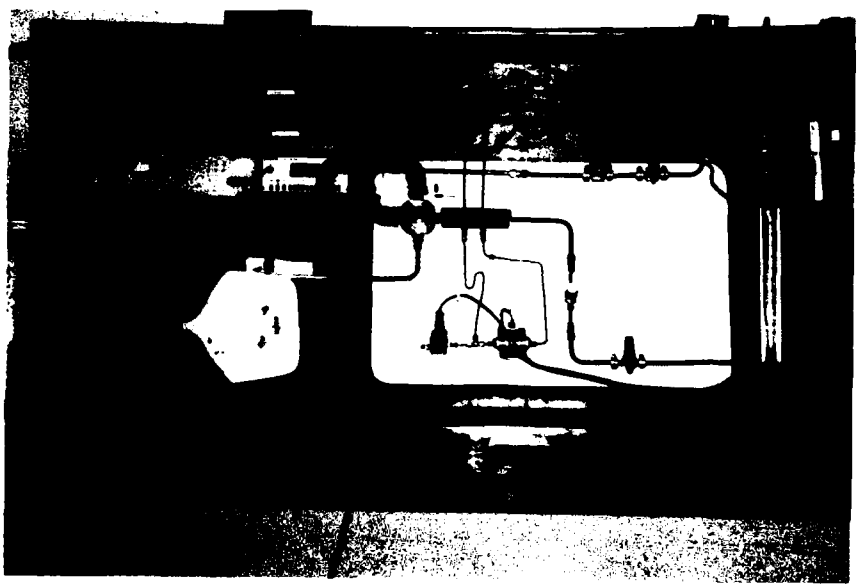

Figure 3.2. Photograph of Test Apparatus

As mentioned in Chapter I, 250 and 325 mesh screen was used so that the results could augment earlier results at NIST. The NIST tests were performed on 200 mesh screen (the

NIST results were not analyzed in time to be included in this research). The actual material, 304 stainless steel was selected because of screen availability. Both screen mesh sizes were Buffalo Wire Cloth manufactured by Buffalo Wirework Company, Inc. The 250 mesh was plain weave and the 325 mesh was twill weave.

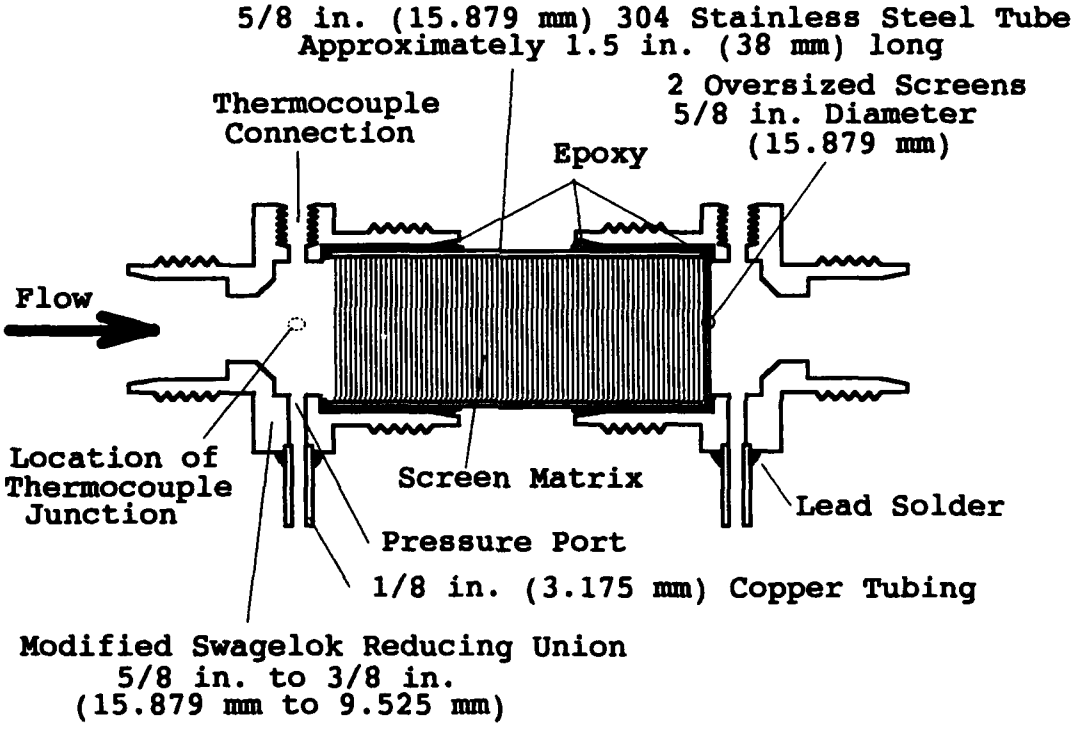

Figure 3.3. Regenerator Schematic

As shown in Fig. 3.3, the regenerator design utilized "off-the-shelf" hardware. The design provided a simple yet easily removed and replaced regenerator. Swagelok brand fittings provided strength and easy installation. In

addition, the regenerator housed the temperature and pressure sample points.

Screen Preparation. Preparing the screen was the most difficult and time consuming task in making the experimental apparatus. The difficulty was primarily due to the unavailability of equipment on Wright Patterson Air Force Base OH, designed specifically to roll material, such as screen, to the precision and repeatability required for this research. The time requirement resulted from the tedious tasks of rolling, cutting, cleaning and packing nearly 5000 screen disks. The next few paragraphs describe the method and equipment used for these tasks.

Screen Rolling. As mentioned above, no equipment was readily available to roll the screen in a precise and repeatable manner. However, after much experimentation, a Milwaukee Horizontal and Vertical Milling Machine, model 205 S-12, proved satisfactory. The machine was used in the horizontal mode.

The moving table of the mill was the key to this application. A standard 1 inch x 4 inch x 24 inch hardened machinist parallel bar was attached to the moving table and used as the rolling surface on which the screen was laid. Next, a hardened steel roller was mounted to the milling machine in place of a cutting tool so that it acted like a rolling pin. The process was similar to rolling dough with a rolling pin, except the rolling pin spun in one position

and the table moved back and forth. Finally, roll fraction was controlled by adjusting the table height.

The method of actually rolling the screen was developed by trial-and-error. The results are as follows:

1. The screen was cut into strips approximately 32 mm x 248 mm (1.25 inch x 9.75 inch).

2. One strip was used as the prototype for its mesh and roll fraction to adjust the table height.

3. Each strip was flatted with four passes of the roller. Before each pass it was flipped either end-for-end or side-to-side. Thus, each corner of the strip was eventually in each corner of the parallel plate.

4. Each strip was checked for thickness with a micrometer in six locations to ensure the thickness was within ± 0.03 mm (± 0.0001 inches).

5. After all the strips of like mesh and percent roll were prepared, they were stored in a large, marked envelope until further use.

A discussion of the effect rolling had on the screen with photographs is included in Chapter IV.

Screen Cutting. Cutting the screen was a relatively simple process, compared to rolling it. The process required a hardened steel punch, a hammer, and a smoothly planed hard maple board. Three strips of rolled screen were laid on top of each other then taped to the board. The punch was placed squarely on top of the screen

and all three strips were punched simultaneously with a hammer. Approximately fifty disks were allowed to back into the tube portion of the punch and then the stack was pushed out of the tube into an appropriately marked bottle. The dimensions of the punch are shown in Fig 3.4.

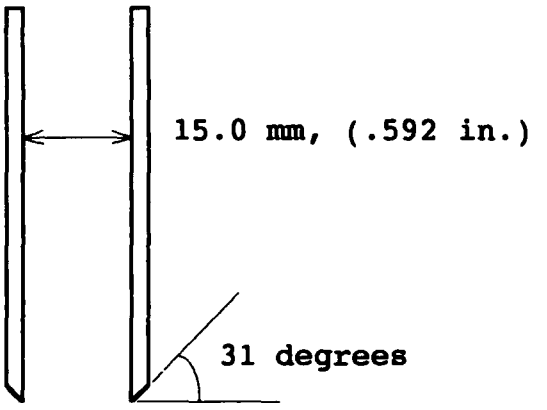

Figure 3.4. Dimensions of Cylindrical Punch Used to Cut Screen Disks

The quantity and quality of the screen disks were closely monitored during the entire process of regenerator assembly. Any unsatisfactory disks were set aside and were subtracted from the total count of disks cut (number of holes x number of layers). Unsatisfactory disks were usually the result of incomplete cutting.

Screen Cleaning. After the screens had been rolled and cut, machine oils and fingerprints were removed. All of the screens of a particular mesh and percentage roll were placed into a glass jar and were completely covered

with acetone. Next, the entire contents was swirled for at least 15 seconds and the acetone discarded. Then, a second batch of clean acetone was added to the still "wet" screen disks and the swirling was repeated. After the second rinse, the acetone was discarded and the screen disks were piled on a heavy duty paper shop towel to air dry. Once dry, latex gloves were used to return the screens to their marked bottle, and the combined mass of the bottle and screen disks was recorded.

Regenerator Assembly. Finally, with the screen prepared, the entire assembly was ready to be completed. The final assembly process spanned at least three days because of the cure times required for the epoxy. Epoxy was selected over lead solder to bond the entire assembly together. This was because of the difficulty in applying lead solder to stainless steel. In addition, silver solder was ruled out, except for the thermocouple assemblies, because of potential heat distortion to the thin stainless steel tube regenerator housing.

As shown in Fig. 3.3 the outlet end of the regenerator contained two oversized screens which were cut using a standard 5/8 inch (15.875 mm) punch. The two screens held the entire stack of screen disks in the tube. The two oversized screens were epoxyed to the flat surface of the brass end cap. The epoxy cured overnight with a glue clamp

firmly pressing the tube against the two oversized screen disks and brass end cap.

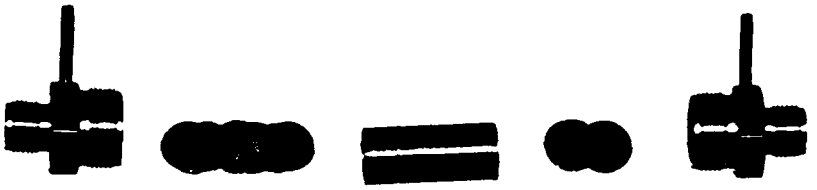

Figure 3.5. Photo of Exploded View of Regenerator

The screen disks were packed into the tube after the epoxy cured overnight. The screen disks were packed in small groups of 10 to 20 by hand using latex gloves. First, a group was picked up and lined up to make a straight, even stack. The entire group was started into the tube end. Next, a push rod [14.6 mm (1.575 inch) diameter] was used to press the group against the previously packed screen disks. After several groups were positioned, force was applied

manually to the rod to ensure the discs were tightly packed. This entire process was continued until no more disks could be placed into the tube. The distance from the top screen to the top of the tube was measured and recorded.

The unused screen disks were counted and returned to their designated bottle. Thus, the number of screen disks packed in each regenerator was calculated from the count made while cutting the screen. In addition, the mass of the bottle with the remaining screen disks was measured, so the mass of screens in the regenerator could be calculated. The accuracy was better than 0.04 percent.

Finally, the regenerator was ready for the final step in the assembly process. The inlet end cap was epoxyed into place, axial pressure was applied with a glue clamp and the epoxy was allowed to cure overnight.

Pressure Test. The final step in the regenerator assembly was to perform a pressure test. This ensured the safety of the regenerator, under the testing pressures of 30 atmospheres. The pressure to the assembly was gradually increased to 34 atmospheres (500 psig). Then, the assembly was checked for leaks using a soap suds solution. Every regenerator assembly passed this test and no leaks were found.

Flow Meter

The flow meter used to measure the mass flow rate of the helium gas was a Brooks Full View Rotameter model 9-1112-10, serial number 6412-75276. The meter was calibrated in standard cubic feet per minute (SCFM) air. The manufacture's calibration plate stated that the $SCFM_{air}$ = 0.1345 x *%scale*. In addition, standard atmosphere was defined as 70 ^{o}F and 0 psig. Equation 2.22 provided the conversion to kg/s of helium from the rotameter scale. The minimum scale reading was 10 percent scale which corresponded to approximately 0.28×10^{-3} kg/s and the graduations were every 2.5 percent. The full scale reading of 100 percent corresponded to approximately 3.2×10^{-3} kg/s.

Pressure Transducers

The system contained three different pressure transducers all of which supplied a voltage to a digital voltmeter so that the readings could be recorded. The three transducers measured inlet pressure, P_1; pressure drop across the regenerator, ΔP; and flow meter pressure, P_{meter}. The next three paragraphs state the range, transducer manufacturer, model, signal conditioner, and digital voltmeter used for each of the three pressure measurements. In addition, the calibration technique and equipment are described. The actual calculations made with these pressure

measurements are included in Chapter II, Theory and Experimental Analysis.

Inlet Pressure, P_1. The P_1 transducer was required to measure the maximum inlet pressure of 30 atm, or roughly 450 psia. A differential pressure was used instead of an absolute pressure transducer because of cost and delivery time. In addition, a digital barometer was readily available so that gage pressure readings could be easily converted to absolute pressure. A Validyne DP15-56, 0-500 psid pressure transducer, serial number 84654, was selected for its accuracy and reasonable cost. It was connected to a Validyne Dual Modulator, CD 280, serial number 109040. The voltage from the CD 280 was measured with a Hewlett Packard HP 3466A Digital Multimeter, serial number 1716A-18320.

Pressure Drop, ΔP. A CEC model 4-351-002, 0 to 50 psid pressure transducer, serial number 2357, was selected to measure the pressure drop through the regenerator. Its range was satisfactory and it was "on-hand". In the process of testing, two transducers failed so a total of three identical transducers were used (the calibration for each transducer was closely tracked). The second and third serial numbers were 2683 and 2769, respectively. In all three cases, the power was supplied with an Endevco Power Supply, model 4225, serial number AG 23; and the signal was amplified with an Endevco Signal Conditioner, model 4423, serial number BA 65. The voltage was displayed on a Hewlett

Packard HP 3466A Digital Multimeter, serial number 1716A-18308.

Flow meter Pressure, P_{meter}. The pressure of the helium entering the flow meter was expected to be slightly above atmospheric pressure because of back pressure from the exhaust tube line. Once again, barometric pressure was readily available so a differential pressure transducer configured for gage pressure was used. A Validyne Differential Pressure Transducer, 0-20 psid, model DP-10-42, serial number 74960 was selected. Its range was acceptable and it was compatible with the Validyne Dual Modulator, CD 280, serial number 109040 (same modulator as P_1, but different channel). The voltage was displayed on a TSI Voltmeter, Model 1076.

Pressure Calibration. All five pressure transducers were calibrated using dead weight testers. All the associated equipment listed above for each transducer was used during the calibration. The voltage vs. pressure was measured for a total of more than 11 points in the range of interest. The readings were taken as the pressure increased then decreased. An Ametek, Type K Pneumatic Pressure Tester, model HK-500, serial number 79672, used for the P_1 and ΔP transducers. An Ametek, Type K, Pneumatic Dead Weight Pressure Tester model PK2-254WC, serial number 79055 was used for the P_{meter} transducer.

Barometric Pressure. Barometric pressure was recorded from a CEC Transamerica Delaval Digital Barometer model 2500-0103, serial number 258. The barometer display was in millimeters of mercury.

Temperature

Temperature measurement at the regenerator inlet and outlet were a crucial part of this study. The next few paragraphs explain the selection of type T thermocouples and the associated equipment which processed and stored the data. In addition, the software which operated the equipment is explained.

Selection of Type T Thermocouples. Temperature measurements needed to be fast and accurate to measure the transient temperature response which resulted from the step temperature change (T_{fl}-T_i). Thermocouples provided the millisecond response required. Type T (copper-constantan) thermocouples were acceptable for the temperature range used in this experiment. The thermocouples used were Omega Subminiature Quick Disconnect Style Sheathed Thermocouple Probes with exposed junctions, model TMQSS-032(S)-6. The sheath diameter was 0.032 inches (0.813 mm) and the wire diameter was 0.006 inches (0.145 mm). The sheath and wire diameters were adequate enough to allow them to resist the drag affects from the flow. However, the junction and wire

diameters were small enough to provide the required quick response.

Figure 3.6 illustrates the thermocouple assembly. The inlet and outlet assemblies were identical. The inlet and outlet thermocouples were always used in the same position.

A third temperature, T_3, was also measured. A matching subminiature thermocouple was epoxyed into a small hole in a Swagelok 3/8 inch union fitting with "Double Bubble" brand epoxy. The fitting was approximately 120 mm from the four-way valve in the secondary flow.

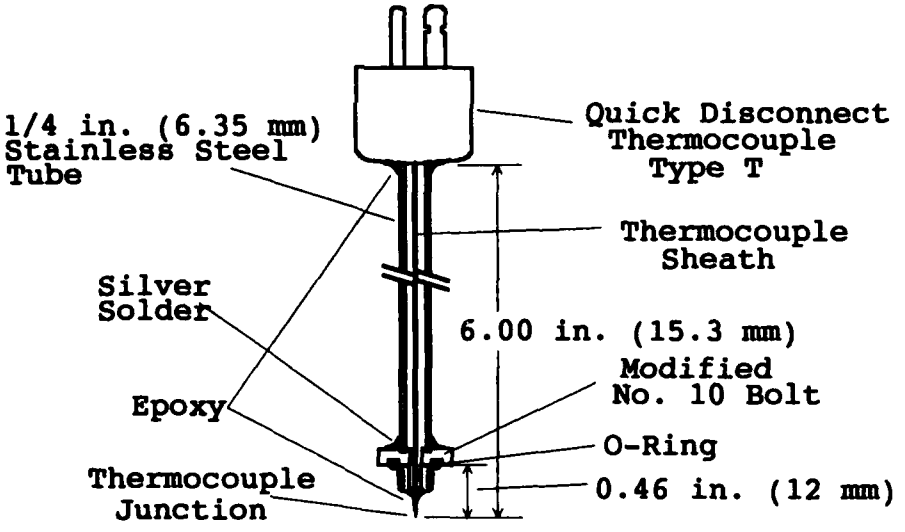

Figure 3.6. Thermocouple Assembly

Signal Processing. Three pieces of equipment were required to process the thermocouple output into

temperature. First, a Keithley MetraByte Corporation EXP-16 16-channel analog multiplexer (serial number 233266) amplified and multiplexed the analog signal for the analog to digital (A/D) converter. The A/D converter was a Keithley MetraByte Corporation DAS-8 12 bit A/D converter (serial number 9537). The DAS-8 was connected to a Zenith Z-248 International Business Machines (IBM) compatible computer.

The manufacturer recommended gain setting, for type T thermocouples, was 200. This included the entire normal operating range of type T thermocouples. The gain resulted in a temperature resolution of 0.3022 K. However, this study was for a much smaller range of temperatures. Thus, the maximum gain of 1000 was used to improve the resolution to 0.0608 K.

Temperature Acquisition Software. The software used to collect the temperature data was written in GW-BASIC 3.20. The manufacturer provided sample software for the user to modify for the user's needs. The program titled "EXP-T.BAS" was the core program used to build the software used for temperature acquisition. This program performed the functions necessary to retrieve temperature data from up to 16 temperature ports in the EXP-16. The program also displayed these temperatures on the computer monitor in real time. The author streamlined and modified the sample software so that it met the specific needs of this study.

The final program (listed in Appendix E) had three modes of operation. The three modes were file initiation, real time display and data acquisition.

The first mode, file initiation, allowed the user to enter the filename of the test which was to be run. The program initiated the matching filenames on the a, b, and c drives of the computer. The program then returned the computer to real time display mode.

The real time display mode displayed the three thermocouple temperatures, the cold junction temperature, the filename, and status of the current file ("old" or "new"). This was the default mode whenever one of the other two modes were not in progress. The other two modes were entered from the real time display mode. This mode allowed the user to know when conditions were favorable to perform a test. It continuously updated and displayed the temperatures until the file initiation or data acquisition mode was selected.

The data acquisition mode was streamlined to maximize the rate of data acquisition. The display of temperatures was no longer updated until an entire test was completed. The following sequence of events occurred. First, the cold junction temperature was recorded (experience showed the cold junction temperature to be steady during the 18 seconds required to collect data). Second, the program entered a loop which stored the clock time and three thermocouple

voltages for each of the 500 readings. Third, the program converted the clock time to elapsed seconds and converted thermocouple voltages to temperatures. The program saved these calculated values to the data file on each disk drive. Finally, the program returned to real time display mode.

Tubing

The factors used to select the type and size of tubing were operating pressure, flow velocity, availability, cost and workability. The tubing had to be pressure rated to at least 30 atm (3 MPa) and have a large enough inside diameter to keep flow velocities low enough to eliminate Mach number compressibility effects (actual maximum velocities were approximately 100 m/s or Mach number equal to 0.1). The considerations of availability, cost and workability all concluded in using copper tubing. Thus, the final selection was 3/8 inch (9.525 mm) outside diameter with 0.032 inch (0.81 mm) wall thickness soft copper tubing.

Valves

The four types of valves used in the test apparatus were a four-way valve, 3 two-way valves, 2 metering valves, and a pressure regulator. All the valves required a pressure rating of at least 30 atm (3 MPa) and had to be sized to allow sufficient flow rates. The sizing criteria was flow coefficient, C_v. The methods of calculating C_v vary slightly between manufacturers. As a results, care was

required when selecting each valve. The next few paragraphs describe the basic conditions for which each valve was selected. The temperature used to find each C_v was 70° F (294 K) but the pressure was the lowest expected at each valve's location.

Four-Way Valve. The four-way valve had to quickly switch the flow to provide the step temperature change required for the experiment. Each channel was sized to allow approximately 3×10^{-3} kg/s flow at an outlet pressure of 10 atm. The valve selected was a Whitey 4-Way Ball Valve, model B-45YF8.

Two-Way Valves. The 3 two way valves allowed quick shut-off and isolation of the system to preserve helium. The two-way valves were sized to allow approximately 3×10^{-3} kg/s flow at 10 atm. The valve selected was a Whitey 2-Way Ball Valve, model B-44S6.

Metering Valves. There were two different metering valves. Both were required to withstand 30 atm differential pressure. The C_v was calculated for 3×10^{-3} kg/s flow at 6.5 atm (to allow for pressure drop experienced upstream in the regenerator). The toughest requirement was to have a smooth, linear response of C_v versus number of turns so that the flow rate could be precisely controlled. The primary flow was controlled with a Nupro Metering Valve, model SS-4BMRG. The secondary flow metering valve had to meet many of the same requirements as the primary valve but was less

expensive. The secondary flow was controlled with a Whitey Screwed Needle Valve, model B-4R56.

Pressure Regulator. The pressure regulator needed to reduce the tank pressure of 2300 psi (16 MPa) to the 10 to 30 atm (150 to 450 psi) range required for the tests. In addition, the valve required a large enough orifice to allow the required total flow rate of approximately 3×10^{-3} kg/s. A Grove 15-L, 3000 psi inlet with 0-750 psi outlet, serial number L-41575 was used.

Ice Bath Design

The cold temperature flow was created by chilling room temperature helium with an ice bath. The heat exchanger surface was made from approximately 3.2 m of tubing rolled into a 0.17 m diameter coil. The tubing was the same type of copper tubing used in the rest of the apparatus. The entire device was housed in a Playmate 18 can cooler. The cooler was filled with ice provided free of charge by the local snack bar.

The ice bath design was based on several simplifying assumptions to estimate the required tubing length. The first assumption was a constant wall temperature of 0 ^{o}C (273 K). The second assumption was a straight tube with laminar flow (worst case). Finally, an entrance temperature of 300 K and an outlet temperature of 274 K was assumed.

Unfortunately, the temperatures entering the regenerator were between 285 K and 290 K.

Helium

The helium was "high purity helium" manufactured by the United States Bureau of Mines, Helium Field Operations. The helium was at least 99.997 percent pure. The helium met the requirements of MIL-P-27407A (Type I, Grade A).

Insulation

Insulation was added to insulate the line between the ice bath and the four-way valve. In addition, a removable section of insulation was placed over the regenerator which extended to the four-way valve. The insulation was standard black foam used for pipe insulation. The foam tube was 3/8 in. (9.5 mm) thick. The insulation was tightly wrapped around the tubing and secured with wire bundle ties to form a seal.

Fittings

All fittings were required to be safe for the operating pressure of 30 atm and to fit the 3/8 inch (9.525 mm) outside diameter copper tubing. In addition, they needed to be able to survive numerous assemblies and disassembles when helium tanks and regenerators were changed. Finally, they were required to accommodate the various valves and other

connections in the system. The final selection was Swagelok brand brass fittings.

Leak Checks

All fittings and connections were checked for leaks upon initial assembly and whenever they were opened or altered in any way. All leak checks were performed by brushing a small amount of soap suds solution over the area in question. Any bubbles or foaming was an indication of a leak and corrective action was taken.

IV. Experimental Results

The previous chapters explained the background, theory and experimental design. These chapters lead to the experimental results. This chapter is divided into three main sections. The first topic is the physical effect that rolling had on the screen. The second topic is the effect rolled screen had on friction. The third topic is the effect rolled screen had on heat transfer. Finally, the combined effects of friction and heat transfer are discussed.

In order to simplify the discussion, the fraction roll, R, is discussed in terms of the approximate values of 0.00, 0.15, 0.30, and 0.50. In actuality, the real values were slightly different for 250 and 325 mesh screens. This simplification eases the comparison between 250 and 325 mesh screen. However, all graphs refer to the actual measured value of R.

Physical Effect of Rolling

The physical effect rolling had on screen is illustrated by scanning electron microscope photographs in Figs. 4.1 and 4.2 (250 and 325 mesh respectively). The first difference between the two figures is that the 250 mesh was plain weave and the 325 mesh was twill weave. This was because of the unavailability of plain weave 325 mesh

Figure 4.1. Scanning Electron Microscope Photos of 250 Mesh Screen at Different Fraction Roll.

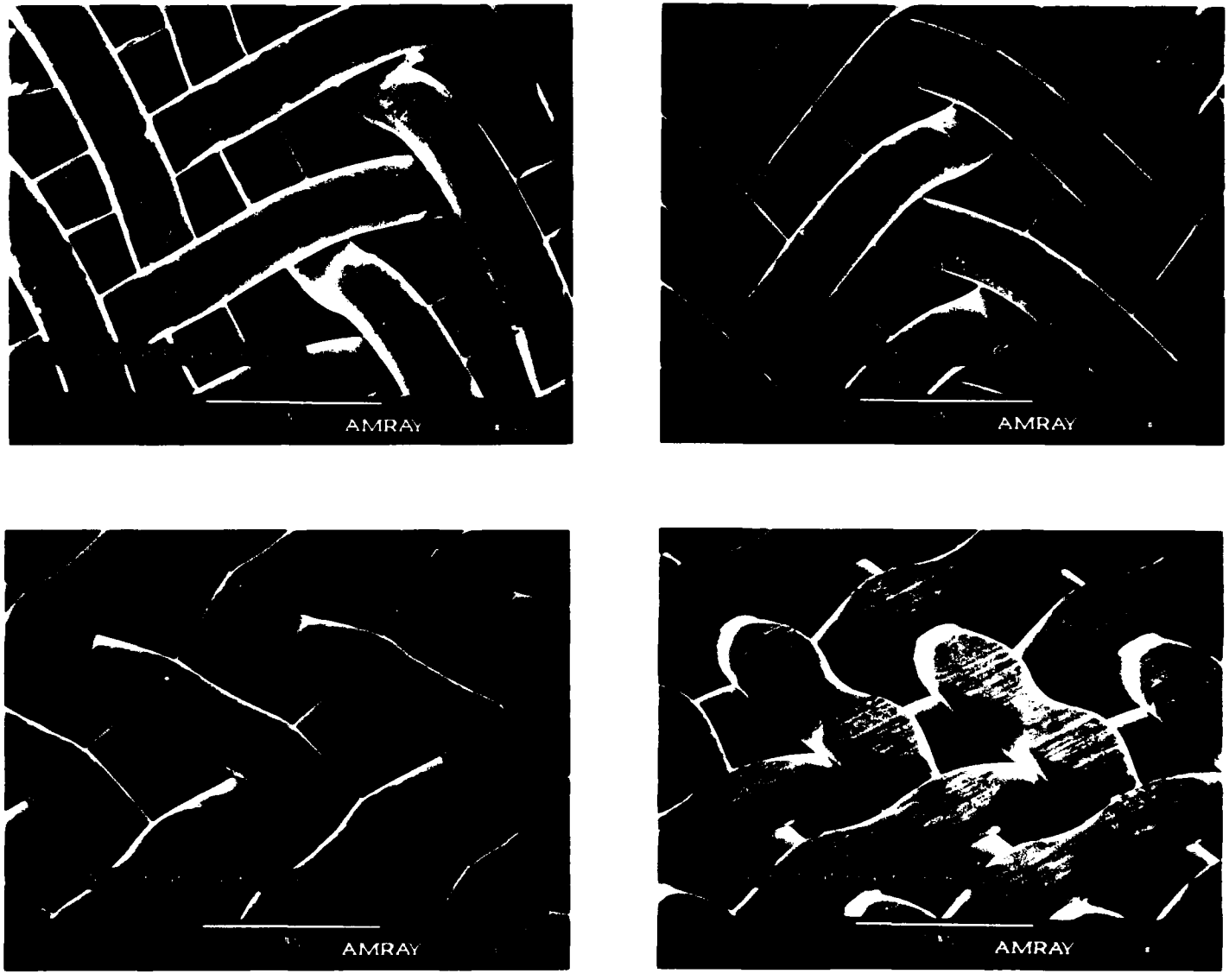

Figure 4.2. Scanning Electron Microscope Photos of 325 Mesh Screen at Different Fraction Roll.

screen. However, both sets of photographs display the same effect due to rolling.

For both the 250 and 325 mesh unrolled (0 fraction roll) screens the cross section of the individual wires was nearly circular in all locations. The effect of rolling was barely evident with the 0.15 fraction roll screen. The distortion was concentrated on the top of each weave resulting in a slight flat spot. However, neither the contact region between crossing wires or the square gap between each weave showed any noticeable change. The 0.30 fraction roll screen demonstrated the same effects as the 0.15 fraction roll except that the flattened region at the top of each weave was larger.

The 0.50 fraction roll screen showed the first signs of large physical distortions due to rolling. First, the flattened region at the top of the weave was significantly larger. Second, there was some distortion in the contact region between crossing wires. Finally, the square gap between each weave was noticeably reduced and no longer had square corners. Thus, the effect of rolling the screen was small for the 0.15 and 0.30 fraction roll screen, but showed significant effect for 0.50 fraction roll.

Friction Results

This section covers the results of the friction measurements. First, the graphical result of friction

factor, f, versus Reynolds number for internal flow, Re, is discussed. Second, the repeatability results are presented. Third, a method to predict friction factor of rolled screen is presented. Fourth, the variation of drag coefficient, C_D, with Reynolds number for external flow, Re_d, is presented to include correlation with previous results. Then, tests from a hollow regenerator are presented. Finally, the overall effect of rolled screen is discussed.

Friction Factor, f. The standard method to present friction results in Kays and London (1984) was the friction factor, f. The investigator used the method in Chapter II to convert the experimental test data to f vs. Re. The next two paragraphs and figures demonstrate sample results from tests with "unchoked" and "choked" flow. Then the combined results showing trends from rolling are presented.

Figure 4.3 illustrates the friction results for the tests of 250 mesh screen with R = 0.15. This figure is an example of tests performed when none of the tests experienced "choked" flow (choked flow is explained in the next paragraph). As Fig. 4.3 illustrates, f is not influenced by variations in inlet pressure. The slight divergence near Re = 100 was the result of random noise since the pattern is not consistent with any of the other series of tests.

Figure 4.4 illustrates the friction results for the tests of 325 mesh and R = 0.50. This figure is an example

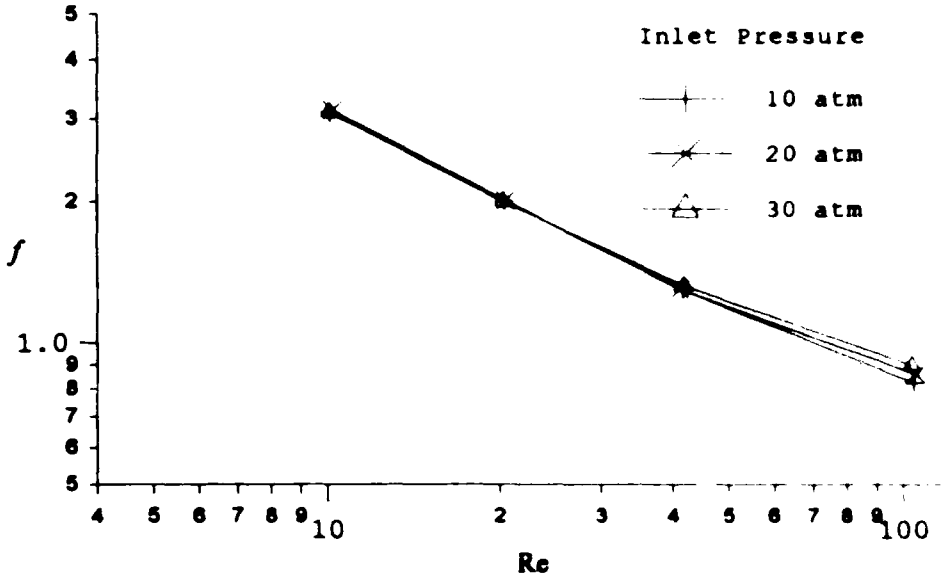

Figure 4.3. Friction Factor, *f*, vs. Reynolds Number, Re, for 250 Mesh Screen with 0.143 Fraction Roll. Uncertainty ranged from 12 percent at the lowest Re and decreased to 1.1 percent at the highest Re for each curve.

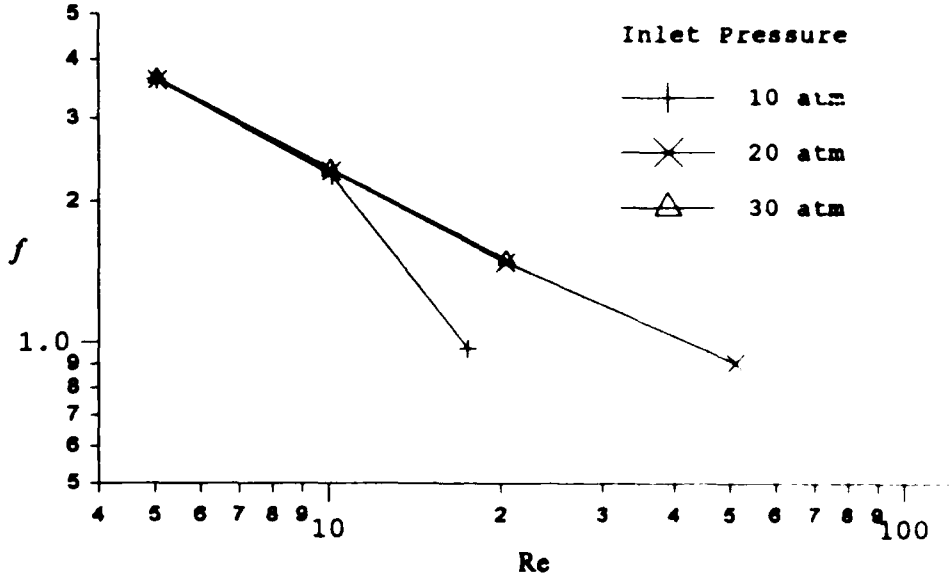

Figure 4.4. Friction Factor, *f*, vs. Reynolds Number, Re, for 325 Mesh Screen with 0.485 Fraction Roll. Uncertainty ranged from 12 percent at the lowest Re and decreased to 1.1 percent at the highest Re for each curve.

of the worst case for choked flow. Choked flow occurred when the pressure drop across the regenerator was such that the flow rate could no longer be increased by opening the flow control valve. The pressures exiting the regenerator in all of the choked flow cases was greater than 3 atm and the system vented to 1 atm. This exit pressure of 3 atm suggests that the flow was not choked by the regenerator itself. Thus, the flow was choked by the smallest orifice in the downstream system which was the flow control valve body. The tests illustrated in Fig. 4.4 experienced choked flow at P_i = 10 and 20 atm. The regenerators which experienced choked flow were 250 mesh R = 0.50; and 325 mesh R = 0.15, 0.30, 0.50. These regenerators experienced choked flow when the inlet pressure was 10 atm. The 325 mesh, R = 0.50 regenerator also choked at 20 atm. In all choked cases, f was lower than the unchoked friction factors.

The trend caused by rolling the screen is shown in Figs. 4.5 and 4.6. In both figures the curves shifted to the left and down as the roll fraction increased. The two basic trends were the shift in both Re and f.

As shown in Chapter II, Re was a function of both mass flow rate, W, and hydraulic radius, r_h. The mass flow rates remained roughly the same for each grouping of data. For example, all regenerators used $W_{min} \approx 0.28 \times 10^{-3}$ kg/s and $W_{max} \approx 2.9 \times 10^{-3}$ kg/s. So, the shift to the left on Figs. 4.5 and 4.6 was due to the decrease in r_h caused by rolling.

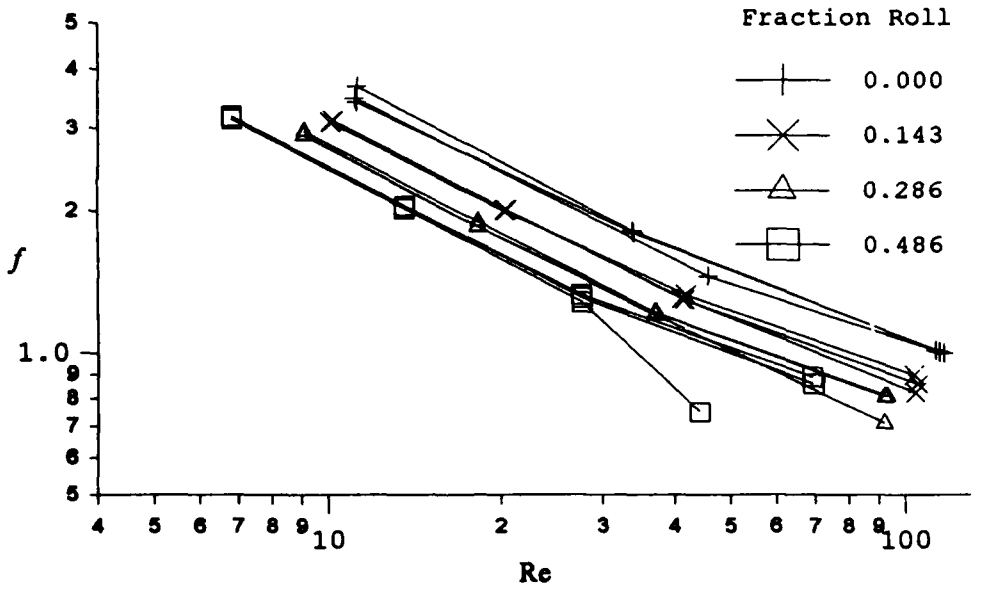

Figure 4.5. Friction Factor, *f*, vs. Reynolds Number, Re, for 250 Mesh Screen. Uncertainty ranged from 12 percent at the lowest Re and decreased to 1.1 percent at the highest Re for each curve.

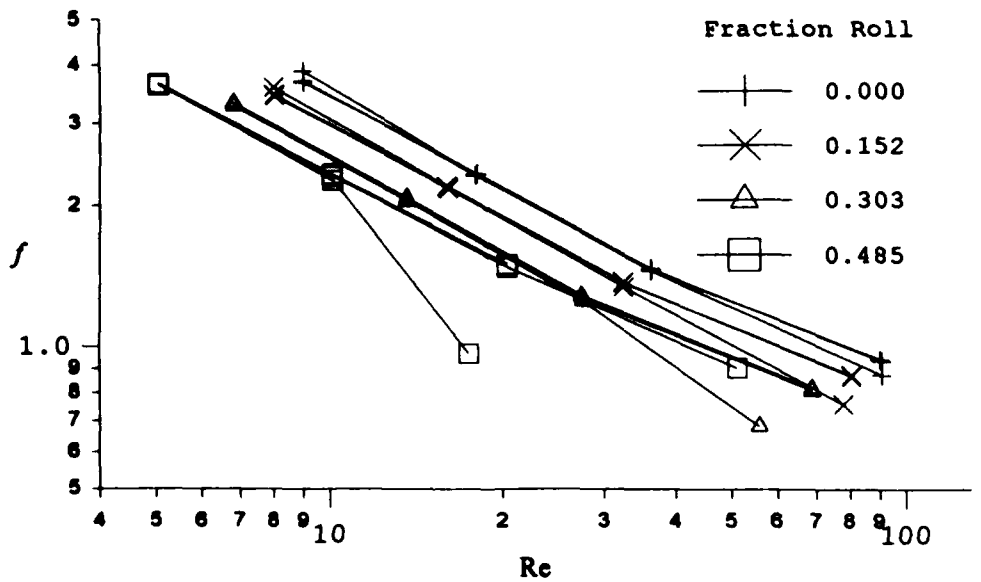

Figure 4.6. Friction Factor, *f*, vs. Reynolds Number, Re, for 325 Mesh Screen. Uncertainty ranged from 12 percent at the lowest Re and decreased to 1.1 percent at the highest Re for each curve.

The decrease in f between regenerators can be misleading. The pressure drop across two different regenerators with the same outside dimensions is not only a function of f, but also the porosity, p, and the total area, A. A method to estimate f and Re is explained in a later section.

Repeatability. The repeatability is illustrated in Fig. 4.7. The repeatability tests were performed using the 250 mesh R = 0.30 regenerator at P_l = 20 atm. The regenerator was connected in the same manner as all other tests. The original data were collected on the same day but the repeat data were collected on two different days. In addition, for each different day's data the 250 mesh R = 0.30 regenerator was freshly reinstalled. As shown in Fig. 4.7, the repeatability was nearly perfect.

Correction Factor for Rolling. The nearly parallel lines in Figs. 4.5 and 4.6 implied that correction of unrolled screen friction factor for rolled screen was possible. The investigator defined the subscript "0" as the property of unrolled screen and no subscript as the property for rolled screen. This resulted in the following definitions:

f = friction factor
f_o = friction factor for unrolled screen
Re = Reynolds number for internal flow at the same mass flow rate as Re_o
Re_o = Reynolds number for internal flow for unrolled screen

p = porosity
p_o = porosity of unrolled screen

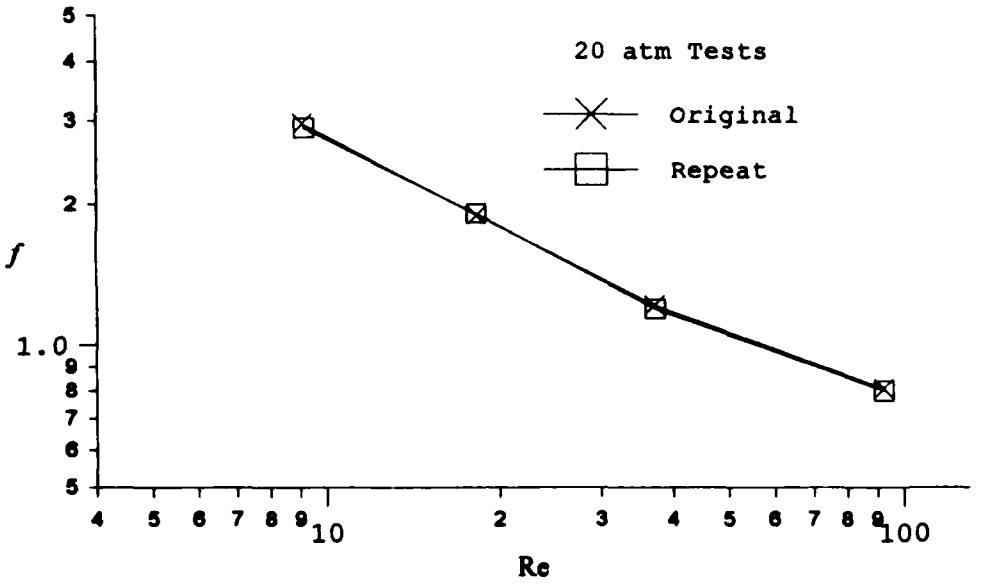

Figure 4.7. Repeatability Test With 250 mesh 0.286 Fraction Roll. Friction Factor, f, vs. Reynolds Number, Re. Uncertainty ranged from 12 percent at the lowest Re and decreased to 1.1 percent at the highest Re for each curve.

The investigator developed a method to normalize the results in Figs. 4.5 and 4.6. The resulting normalized friction factor was fp/f_op_o. Figure 4.8 shows that fp/f_op_o vs. fraction roll, R, converged into a nearly linear relationship. Because the lines of constant Re_o overlaped, the lines were removed and only the data points were plotted.

The six circled points in Fig. 4.8 were all at P_1 = 10 atm and at the highest flow rate tested. Four of the six circled points were at the choked flow conditions

mentioned previously and the other two were measured at the maximum flow rate of 2.9 x 10^{-3} kg/s.

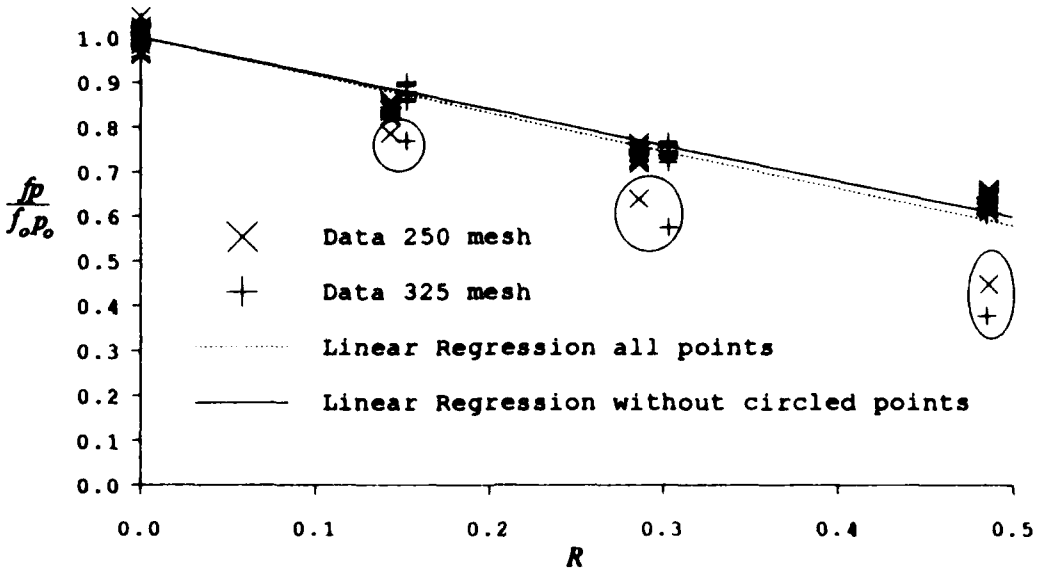

Figure 4.8. Normalized Friction Factor vs. Fraction Roll, R

Figure 4.8 depicts two different linear regressions. The first line was with the six circled points and the second was without the six circled points. The regression was performed so that the intercept of the vertical axis was forced to equal one. The resulting equations were

$$\frac{fp}{f_o P_o} = 1 - 0.845R, \text{ all points} \qquad (4.1)$$

$$\frac{fp}{f_o P_o} = 1 - 0.804R, \text{ without circled points} \qquad (4.2)$$

Estimation Technique for f. For 250 and 325 mesh, the investigator developed the following process to calculate f: First, calculate Re_o from properties of unrolled screen using Eq. 2.23. Second, calculate f_o by multiplying C_D (improved curve fit , Eq. 4.5, or some other source) by f/C_D (Eq. 2.5). When calculating f_o use Re_o and p_o. Third, either measure p if the regenerator is already constructed or approximate it using $p \approx p_o(1+R)-R$ [derived from definitions of p (Eq. 2.15) and R (Eq. 2.18) assuming perfect regenerator packing]. Fourth, apply Eq. 4.1 or 4.2 to calculate f. Finally, if Re is desired it can be approximated as $Re \approx Re_o(1-R)$ assuming that the screen can be perfectly and evenly packed.

This technique is useful for calculating f for the parameters of this research (250/325 mesh, $10 < Re_o < 100$ and $R < 0.50$ for helium gas). However, the investigator expects this technique could be extrapolated to other mesh sizes, gases, and Reynolds numbers.

Comparison to Previous Research. As discussed in Chapter II, Tong and London (1957) provided the following empirical curve fit for screen matrixes:

$$\log_{10} C_D = \frac{1.33}{p^2} Re_d^{-0.33} - \frac{0.54}{p}. \qquad (2.4)$$

where

C_D = drag coefficient per screen
Re_d = Reynolds number for external flow (Eq. 2.24)

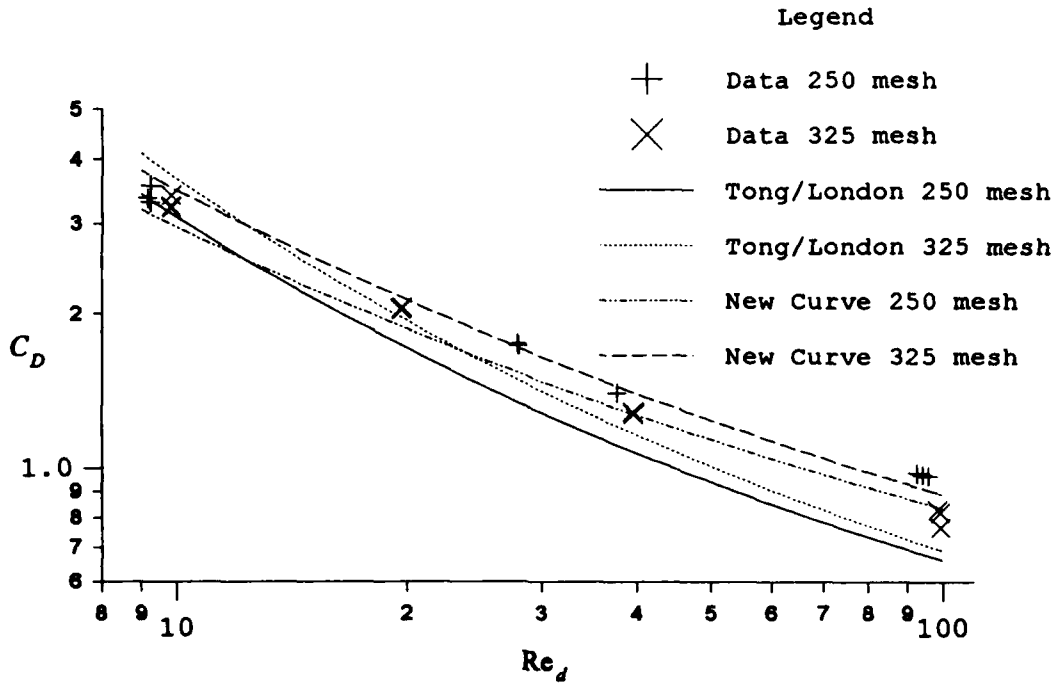

Figure 4.9. Comparison to the Curve Fit of Tong and London (1957). Drag coefficient, C_D, vs. Reynolds Number. Re_d. Uncertainty ranged from 12 percent at the lowest Re_d and decreased to 1.1 percent at the highest Re_d for each curve.

The Tong and London (1957) curve fit is plotted on Fig. 4.9 with the data for unrolled screen. The agreement was good. The Tong and London (1957) data was taken with air using a significantly larger matrix of crossed rods and corrected for woven screen.

A correction to the curve fit of Tong and London (1957) was applied by using an equation of the form

$$\log_{10} C_D = \frac{A_o}{p^2} Re_d^{B_o} + \frac{C_o}{p}. \qquad (4.3)$$

The constants A_o, B_o, and C_o were to be found. A standard least squares technique (Strang, 1988:154) could not be

applied to solve for all three constants simultaneously. This was because the right hand side of Eq. 4.3 could not be separated into linearly independent terms. The investigator attempted several iteration techniques but the best solution was found by assuming Tong and London's value of C_o = -0.54. This resulted in a linear regression of

$$\log_{10}\left(p^2 \log_{10} C_D - pC_o\right) = \log_{10} A_o + B_o \log_{10} \mathrm{Re}_d \,. \qquad (4.4)$$

Thus, the linear regression of Eq. 4.4 using unrolled screen data provided the new curve fit

$$\log_{10} C_D = \frac{1.10}{p^2} \mathrm{Re}_d^{-0.254} - \frac{0.54}{p} \,. \qquad (4.5)$$

As is shown in the next section, this relation holds for $R \leq 0.30$ using $p = p_o$. The new curve fit is also plotted on Fig. 4.9.

Drag Coefficient Results. The drag coefficient, C_D, was calculated by converting the friction factor, f, to C_D using Eq. 2.5. In addition, the Reynolds number for external flow, Re_d, was calculated using Eq. 2.24. Re_d remained constant for a particular flow rate, W, and mesh size. Figs. 4.10 and 4.11 are the resulting graphs.

The 250 mesh results in Fig. 4.10 are quite interesting. For R up to 0.30 the drag coefficient was unchanged. In addition, for 325 mesh screen (Fig. 4.11) C_D was unchanged for R = 0.15 and it increased slightly for R = 0.30. This means that for the two mesh sizes considered the screen can be rolled up to R = 0.30 without any

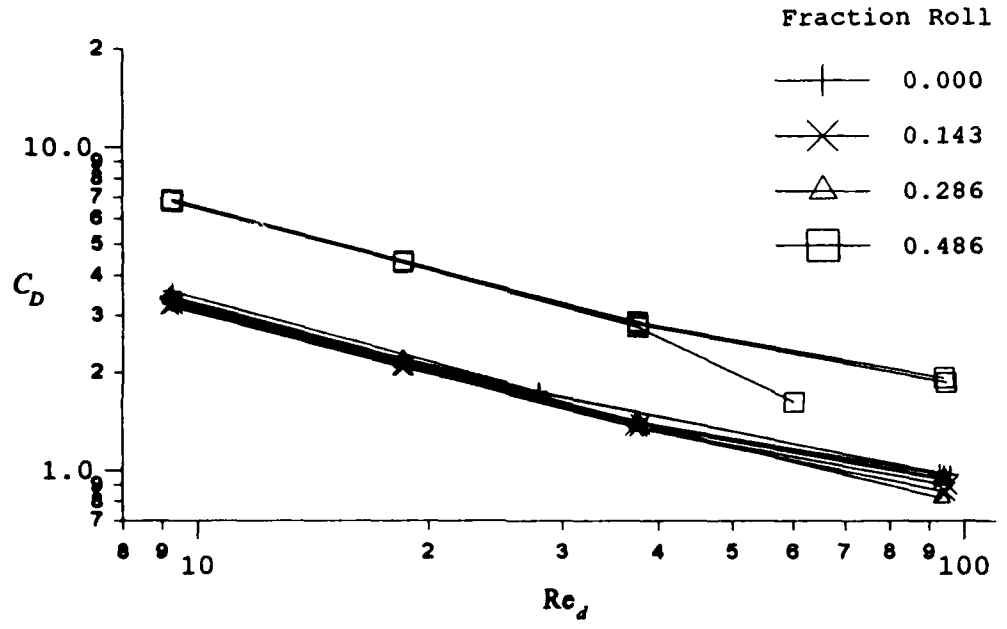

Figure 4.10. Drag coefficient, C_D, vs. Reynolds Number, Re_d, for 250 mesh screen. Uncertainty ranged from 12 percent at the lowest Re_d and decreased to 1.1 percent at the highest Re_d for each curve.

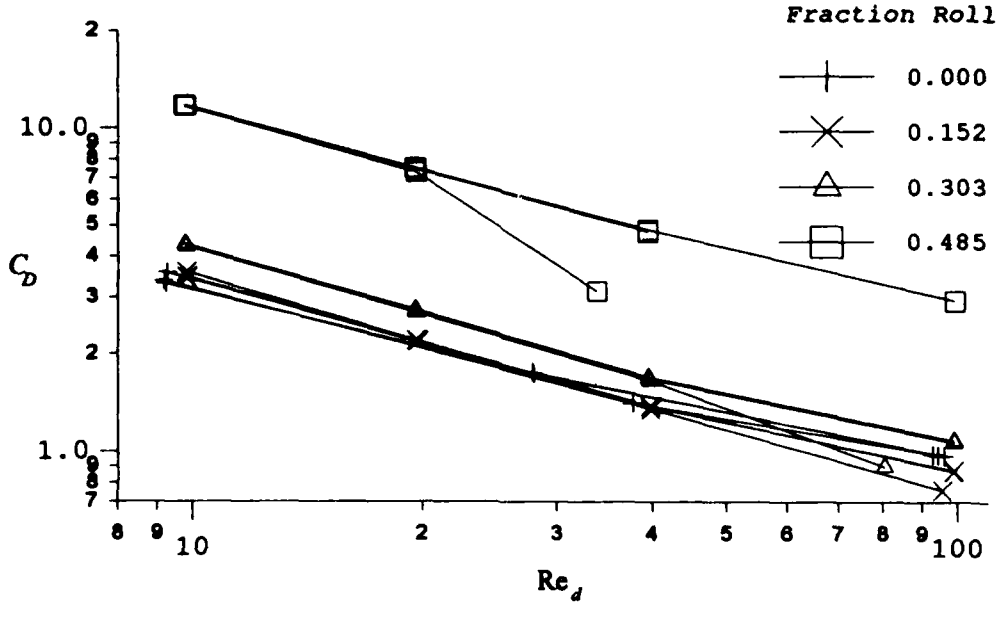

Figure 4.11. Drag coefficient, C_D, vs. Reynolds Number, Re_d, for 325 mesh screen. Uncertainty ranged from 12 percent at the lowest Re_d and decreased to 1.1 percent at the highest Re_d for each curve.

noticeable change in C_D. C_D is discussed further in the friction discussion.

Empty Tube Tests. Tests were performed on an empty tube which was constructed in the same manner as the other regenerators. The only difference was that screen disks were not added. The four tests were performed at P_1 = 10 and 30 atm and W = 0.28 x 10^{-3} and 2.9 x 10^{-3} kg/s. Thus, the empty tube tests were performed at the minimum and maximum extremes of the test conditions. The pressure drop was compared to the unrolled 250 mesh results at matching P_1 and W. The ΔP was between 0.2 and 0.4 percent of the 250 mesh results. Thus, the design of the regenerator case had a minimal effect on the test results.

Friction Discussion. As was discussed earlier, the friction factor for 250 and 325 mesh screen can now be predicted for 10 < Re_o < 100 (Eq. 4.5 and Eq. 2.18). The new Reynolds number after rolling can also be predicted, $Re = Re_o(1-R)$. However, these values do not provide a good intuitive relationship for predicting the pressure drop for a regenerator with rolled screen.

Re_d and C_D seem to be superior to Re and f for correlation. The advantage to Re_d is that it is uninfluenced by porosity where Re is influenced. Because C_D is constant for $R \leq 0.30$, the pressure drop across a given number of screens will be constant whether the screens have

been rolled or not. Thus, C_D is more useful than f which does not remain constant.

Heat Transfer

This section presents the heat transfer results for the research. First, the graphical results of Colburn factor, j_H, versus Reynolds number for internal flow, Re, are discussed. Then, the repeatability results are presented. Next, an approximate method to predict the Colburn factor for screen is presented for varied amounts of rolling. The results for tests with a hollow tube are also discussed. In addition, the actual convection heat transfer coefficient, h, is plotted. Finally, the overall results are discussed.

Colburn Factor, j_H. Figure 4.12 is an example of the test results for a regenerator. The test results were for 250 mesh with 0.15 fraction roll. This figure shows that the heat transfer results were not as tightly grouped as the friction results. In addition, the curve shows j_H was independent of inlet pressure because the results were randomly scattered around the basic trend. Since there was no noticeable trend for tests with choked flow, there is no figure showing this data.

Figures 4.13 and 4.14 illustrate the overall trend of rolling on j_H vs. Re. In order to simplify the appearance of the graphs the data points were not connected as the friction graphs were. Instead, the solid lines represent a

curve fit of the results for all the data for a particular regenerator. These curve fits were made by performing a quadratic curve fit to the logarithms of j_H and Re.

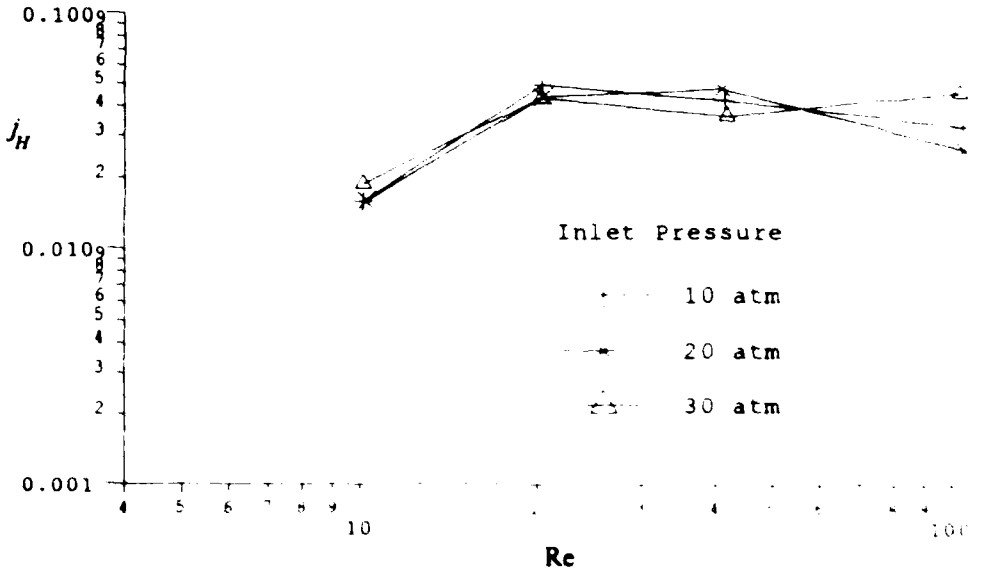

Figure 4.12. Sample Test Results Using 250 Mesh 0.143 Fraction Roll. Colburn Factor, j_H, vs. Reynolds Number, Re, for 325 mesh screen. Uncertainty ranged from 15 percent at the lowest Re and increased to 50 percent at the highest Re for each curve.

Like the friction results, the curves shifted down and to the left with increasing fraction roll, R. As explained in the friction section, the shift to the left on the graph was due to the decreasing hydraulic radius, r_h, reducing Re. A method to predict j_H is presented in a later section and the results are further discussed with the aid of plots of convection heat transfer coefficient.

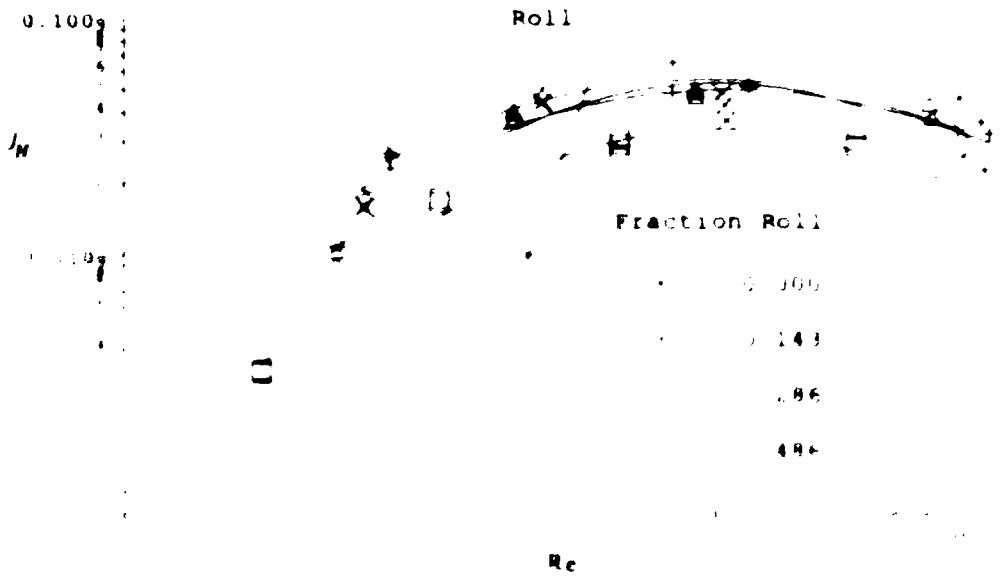

Figure 4.13. Colburn Factor, j_H, vs Reynolds Number, Re, for 250 Mesh Screen. Uncertainty ranged from 15 percent at the lowest Re and increased to 50 percent at the highest Re for each curve.

Figure 4.14. Colburn Factor, j_H, vs Reynolds Number, Re, for 325 Mesh Screen. Uncertainty ranged from 15 percent at the lowest Re and increased to 50 percent at the highest Re for each curve.

__Repeatability__. The repeatability tests for heat transfer were run simultaneously with the friction repeatability tests. The tests were performed on 250 mesh screen with 0.30 fraction roll at 20 atm inlet pressure. The original tests were conducted on the same day but the repeat tests were performed on two different days. The results of these tests are illustrated in Fig. 4.15. The repeatability was not as outstanding as the friction tests, but the results showed reasonable repeatability.

__Comparison to Previous Research__. As discussed in Chapter II, Tong and London (1957) performed tests for woven screen matrices. Their curve fit is Eq. (2.[illegible]). Figure 4.16 illustrates the curve fit from Tong and London compared to the results from the unrolled screen. These results were not nearly as compatible as the friction results. At low Re the results of this research and Tong and London (1957) were an order of magnitude different. In addition, at low Re the Colburn factor [illegible] increased as Re increased which is reversed from the trend of Tong and London (1957).

The differences from Tong and London [illegible]

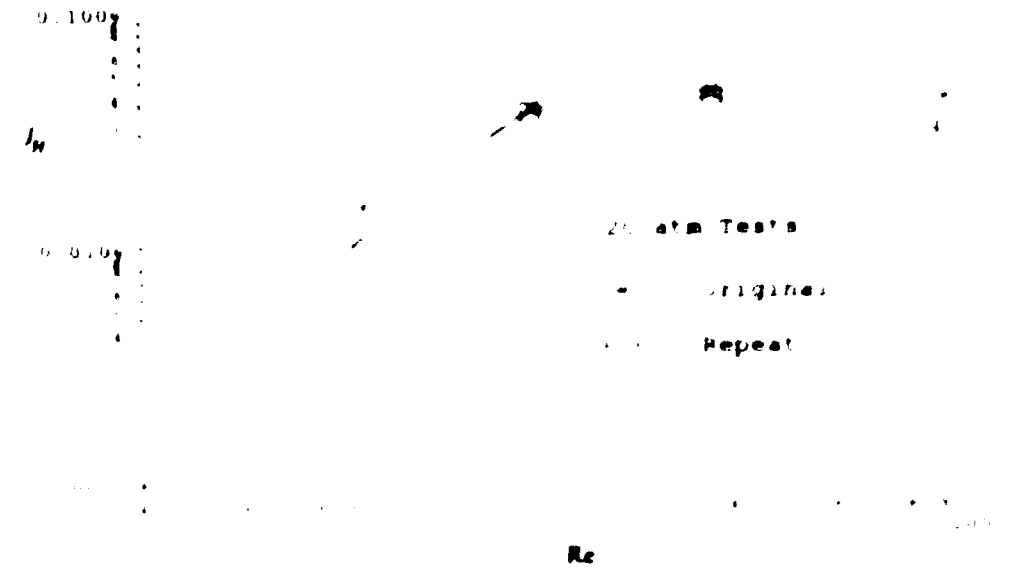

Figure 4 15 Repeatability Using 250 Mesh 0.143 Fraction Roll Colburn Factor, j_H, vs Reynolds Number, Re. Uncertainty ranged from 15 percent at the lowest Re and increased to 50 percent at the highest Re for each curve.

helium gas. Finally, the range of Re for this research was $9 < Re < 110$ and Tong and London had a much larger range of $5 < Re < 100{,}000$.

The data for this research did not have the same functional form as Tong and London's data, thus a new function was sought. The new curve fits for unrolled screen are

$$\ln j_H = -9.7 + 3.7\ln(Re) - 0.51(\ln(Re))^2 \quad (250 \text{ mesh}). \tag{4.6}$$

$$\ln j_H = -11.2 + 4.6\ln(Re) - 0.63(\ln(Re))^2 \quad (325 \text{ mesh}). \tag{4.7}$$

Approximation for j_H. Attempts to normalize j_H as was done with friction, f, were not as successful. Numerous methods of normalization were tried including ratios of porosity, p; total heat transfer area, A; minimum free-flow area, A_c; and combinations of these ratios. The least scatter in the results resulted in the normalization $(j_H A_o)/(j_{Ho} A)$. The investigator defined j_{Ho} as the Colburn factor for unrolled screen and A_o as the total heat transfer area for unrolled screen. Figure 4.17 illustrates the results of this normalization. Notice that the five points significantly above the other points were all for 250 mesh screen. This occurred at the maximum flow rate of approximately 2.9×10^{-3} kg/s. The inlet pressures were 20 and 10 atm. The linear regression for all the data was

$$\frac{j_H A_o}{j_{Ho} A} = 1.04 \tag{4.8}$$

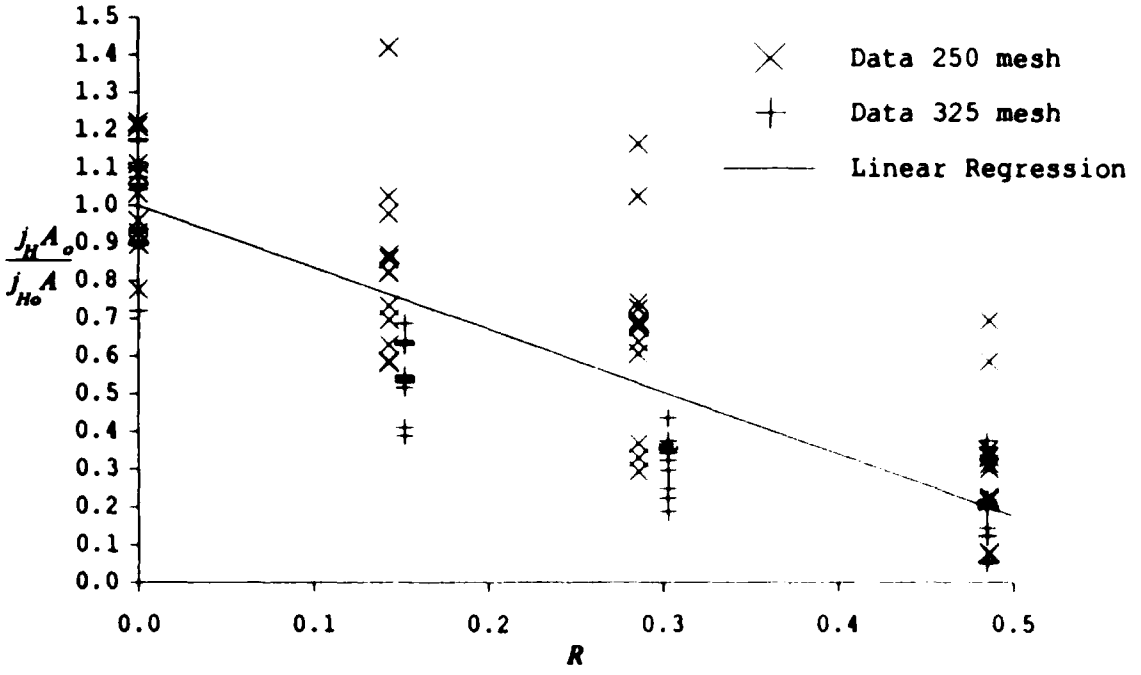

Figure 4.17. Normalized Colburn Factor vs. Fraction Roll, *R*

The methodology to determine friction factor, f, (Eqs. 4.1 and 4.2) applies to determine j_H using Eq. 4.8. The Colburn factor for unrolled screen, j_{Ho}, can be found with Eq. 4.6 or 4.7.

Convection Heat Transfer Coefficient. All the work with Colburn factor, j_H, was aimed at finding the convection heat transfer coefficient, h. The dimensionless terms are extremely useful because they can be applied to multiple situations. However, the meaning of the data can easily become obscured. For this reason h, for the specific case of this research, is illustrated in Figs. 4.18 and 4.19. Although the specific numbers only apply to the regenerators of this research, the trend from rolling the screen is

clear. At low flow rates the convection heat transfer coefficient decreased an order of magnitude as R was increased from 0 to 0.50. As the flow rate increased the difference between rolled and unrolled screen decreased. In fact, the results for R = 0.50 showed h actually becoming higher. Therefore, at low flow rates rolling the screen was detrimental to h and at higher flow rates the differences became less significant. These results are generalized in the heat transfer discussion.

Empty Tube Tests. Tests were performed on an empty tube that was constructed in the same manner as the other regenerators except that screen disks were not added. The tests were performed at the minimum and maximum flow rates of this research (0.28×10^{-3} and 2.9×10^{-3} kg/s, respectively). For each flow rate the inlet pressure was 10 and 30 atm. Thus, a total of four tests were performed at the extreme conditions of the testing. At each flow rate the transient temperature response was recorded with the same method as all of the other tests.

The results were independent of inlet pressure so only one test from each flow rate is shown in Fig. 4.20. Figure 4.20 provides a comparison between the empty tube's transient response and unrolled 250 mesh response. The flow rate and inlet pressure were the same. The comparison was done with the unrolled 250 mesh regenerator because its screens had the smallest mass and total heat transfer area

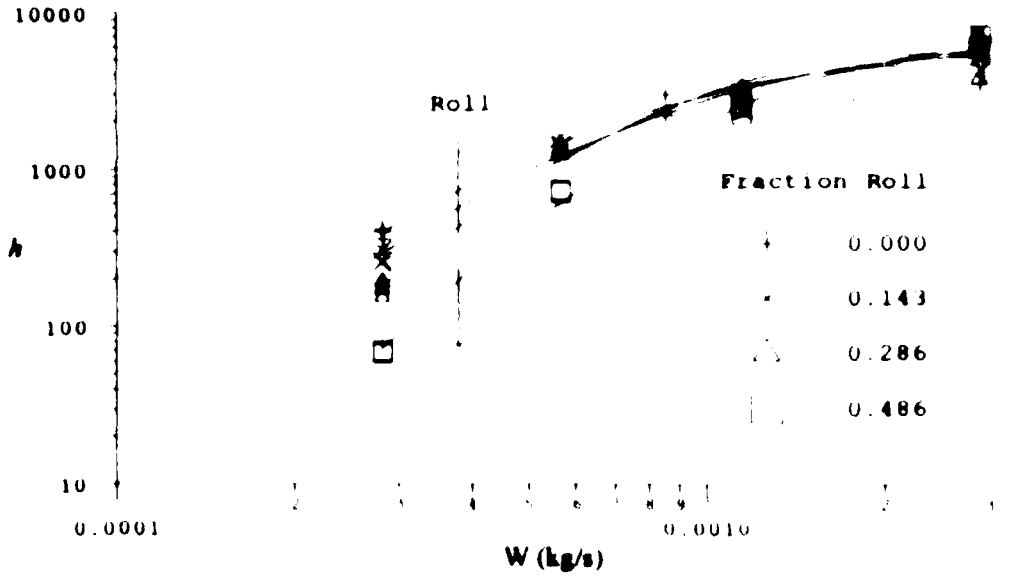

Figure 4.18 Convection Heat Transfer Coefficient, *h*, vs. Flow Rate, *W*, for 250 Mesh. Uncertainty ranged from 15 percent at the lowest *W* and increased to 50 percent at the highest *W* for each curve.

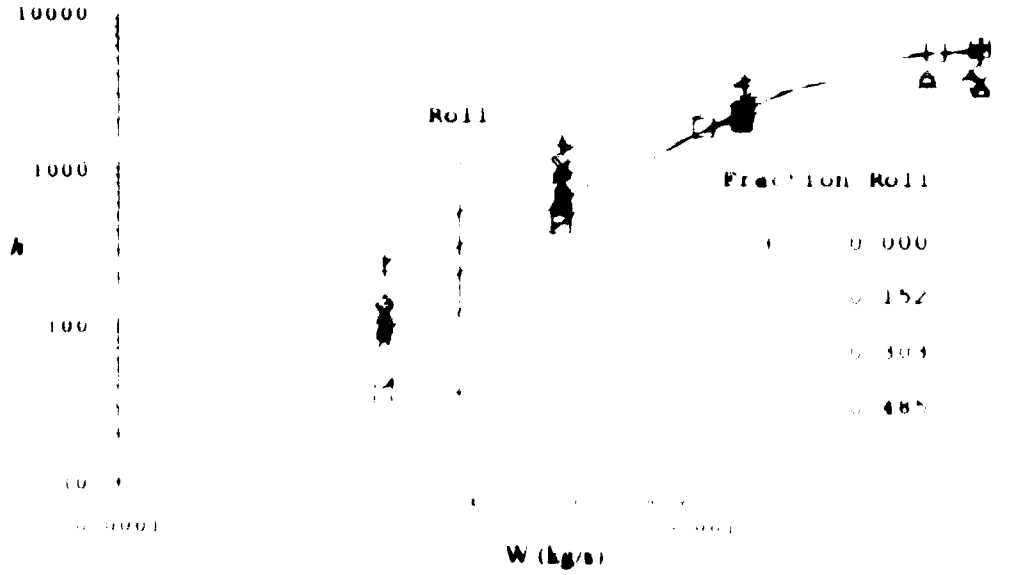

Figure 4.19 Convection Heat Transfer Coefficient, *h*, vs. Flow Rate, *W*, for 325 Mesh Uncertainty ranged from 15 percent at the lowest *W* and increased to 50 percent at the highest *W* for each curve

For this reason, it would be most likely to be affected by the regenerator case. Figure 4.20a shows the lowest flow rate. The empty tube had an outlet temperature T_2 which remained roughly 0.5 K higher than the inlet temperature, T_1. But, the important point is to compare the slope of T_2 vs. time between 7 and 8 seconds for the empty tube and regenerator. During this time interval the slope of the regenerator (right hand graph) was much steeper than for the empty tube. The *maximum slope* used to calculate the number of heat transfer units, N_{tu}, for the regenerator was measured within this time interval. Thus, the regenerator case caused a minimal effect on the slope measurement for the regenerator. A similar comparison is true for the high flow rate tests shown in Fig. 4.20a. The only difference in the figure is the that the time elapsed after the drop in T_1 is the important interval for the slope comparison. Thus, the results of the empty tube tests showed that the regenerator case had a minimal effect on the measurement of *maximum slope*, i.e. heat transfer.

Heat Transfer Discussion. As was discussed earlier, the Colburn factor, j_H, and Reynolds number, Re, both decreased as the screen was rolled. A rough approximation of j_H can be made using a normalization of Colburn factor (Eq. 4.8). Unfortunately, the differences between the previous results of Tong and London (1957) did not allow the investigator to use their method to provide an improved

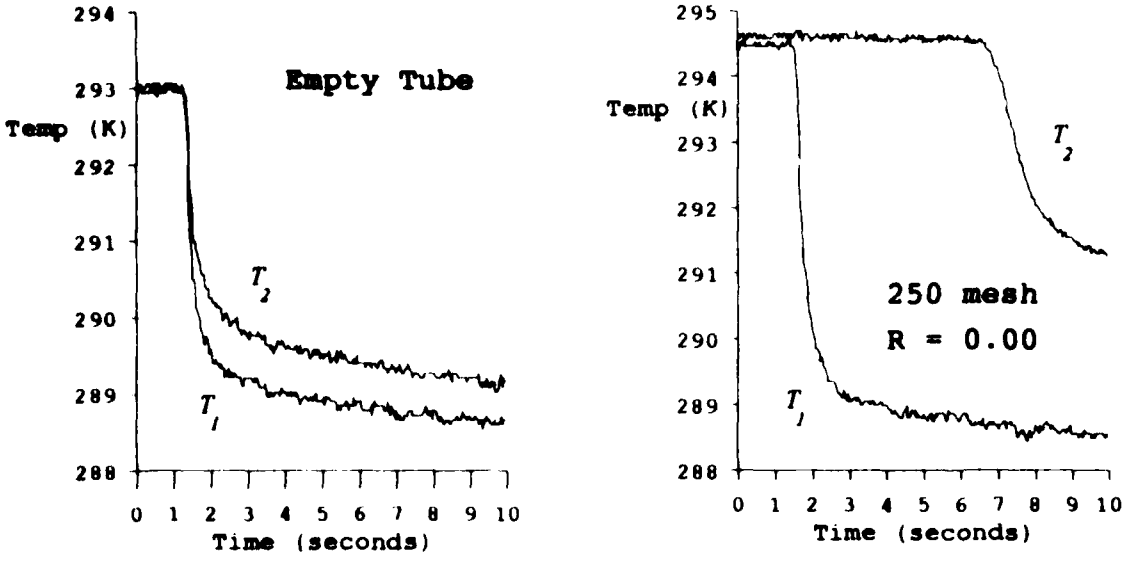

Figure 4.20a. Comparison of Transient Response of the Empty Tube and Unrolled 250 Mesh Regenerator at 0.28 x 10^{-3} kg/s

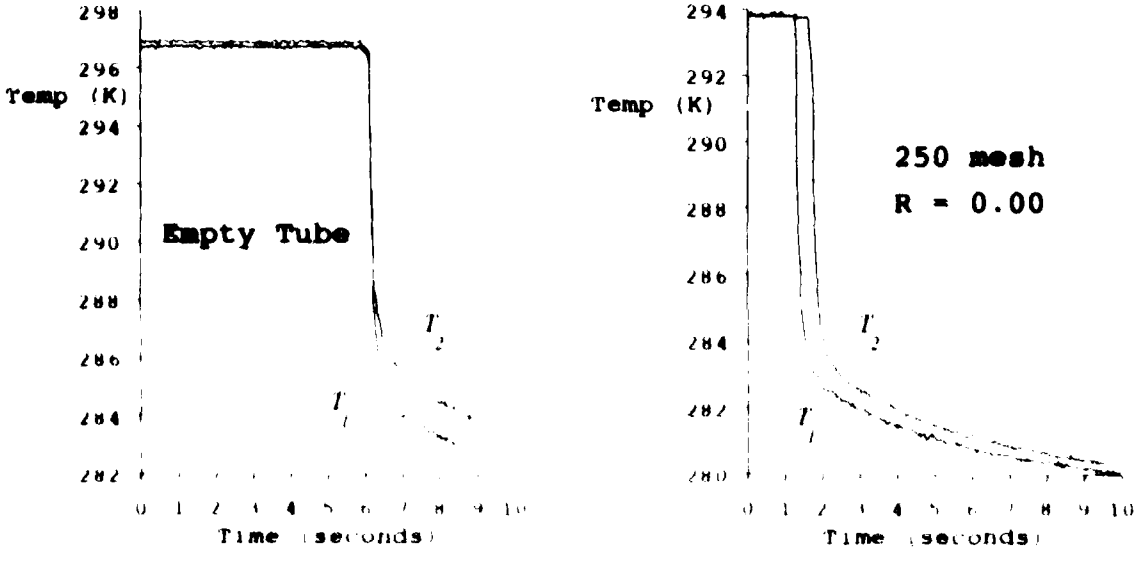

Figure 4.20b. Comparison of Transient Response of the Empty Tube and Unrolled 250 Mesh Regenerator at 2.9 x 10^{-3} kg/s

curve fit. Furthermore, an intuitive understanding of the actual change in heat transfer abilities can be lost in the dimensionless value j_H.

The actual convection heat transfer coefficient, h, for the test results provided some insight to the heat transfer. The observations from the specific values of h vs. W in Figs. 4.18 and 4.19 can be applied to general cases. For $Re_o < 40$, rolled screen demonstrated significantly reduced heat transfer. But for $40 < Re_o < 100$, the difference was less pronounced. The trend in the range of Reynolds numbers tested suggested that the heat transfer could actually show negligible differences for rolled screen as Re_o is increased beyond 100.

Discussion of Friction and Heat Transfer

The effects of rolled screen on friction and heat transfer were discussed separately in prior sections. Now the combined effects of both will be discussed together. Recall the term Re_o is the Reynolds number for internal flow based on the properties of unrolled screen.

Friction and heat transfer provided somewhat opposing conclusions. First, the drag coefficient per screen, C_D, remained mostly unchanged for screens rolled to $R \approx 0.30$. Though, between $R = 0.30$ and $R = 0.50$ an increase in C_D was noticed. However, heat transfer provided a very different conclusion. Any amount of rolling caused noticeable

reductions in heat transfer, especially for $Re_o < 40$. As Re_o increased, the relative reduction in heat transfer for rolled screen became less significant. The most interesting result was for $R = 0.50$ at the highest mass flow rates. At these conditions, h was the same as the unrolled screen (this favorable observation could be negated by the increased pressure loses at $R = 0.50$). In addition, for $40 < Re_o < 100$ the relative difference in the heat transfer was smaller than the uncertainty range of the experiments. So, the data curves show a difference in heat transfer due to rolling. However, the uncertainty is large enough that no conclusions can be drawn for $40 < Re_o < 100$.

For $Re_o < 40$ heat transfer ability decreased as the screen was rolled. The drag coefficient per screen, C_D, was unchanged for $R \leq 0.30$. So, to obtain a required heat transfer rate, more layers of screen may be needed (increasing total area, A). This in turn would result in an increase in pressure drop across the regenerator. Thus, in the region of low Re_o and low R, there appears to be no advantage to rolled screens.

The relative loss in heat transfer ability due to rolling diminished as Re_o increased. For $Re_o \approx 100$ the heat transfer became the same for rolled screen as for unrolled screen. In addition, the friction results did not indicate an increase in friction with increased rolling for up to 0.30 fraction roll. Therefore, tests in the region $Re_o \approx 100$

and $R \leq 0.30$ showed the friction and heat transfer properties were unaffected by rolling. Thus the data in the region $Re_o \approx 100$ and $R \leq 0.30$ suggest that tests for $Re_o > 100$ would be beneficial.

The combined effect of heat transfer and friction when considered with the dead space of a complete cryocooler is worth evaluating. This could most likely be accomplished with the aid of the numerical model "Regen 3.1" developed by Gary and Radebaugh (1991) which was mentioned in Chapter I.

V. Conclusion and Recommendations

This chapter contains two sections. First, the bottom line of the results is stated in the conclusion. Second, recommendation for future research and improvements to the test apparatus are listed.

Conclusion

As the screen was rolled, Re and f decreased. The graphs of C_f vs. Re_d showed that for fraction roll up to 0.30 the drag coefficient was unchanged. Thus, the friction results suggested that the screen thickness can be reduced by as much as 30 percent without increasing the pressure drop for a fixed mass flow rate and fixed number of screens.

In the region $Re_o < 40$, the heat transfer (j_H and h) was decreased an order of magnitude as the roll fraction was increased to 0.50. In the region $40 < Re_o < 100$, the reduction in j_H and h due to rolling became less pronounced.

Combining the trends of the heat transfer and friction results suggests that for $Re_o > 100$ rolled screen may perform the same as unrolled screen. But, tests were not performed for $Re_o > 100$ due to limitations in the present test apparatus. Thus, future research for $Re_o > 100$ could prove rolled screen to be a practical approach to reducing the void volume.

Recommendations

Recommended areas for extended research include:

1. Perform tests on rolled screen for Re using smaller diameter regenerators. Maintain the same flow rates so that most of the same apparatus may be used and the helium usage may be minimized.

2. Apply the friction and heat transfer results from this research to a Stirling cycle model. This will answer the question of the conflicting gain from reduced void volume and loss from reduced heat transfer. A possible model is "Regen 3.1" (Gary and Radebaugh 1991).

Recommended improvements to the test apparatus include:

1. Improve the accuracy of the transient temperature measurements, since these measurements were the limiting factor to the heat transfer calculations. This can be done with a high speed temperature data acquisition hardware and software package.

2. More closely approximate a step temperature change by removing the thermal effect of the tubing in critical areas.

3. Increase the size of the step temperature change by improving the ice bath, because the change was only half of the desired 20 K drop.

Appendix A: Properties of Helium and 304 Stainless Steel

Table A.1 Properties of Helium

Properties of He4 at P = 101.325 kPa

M = 4.003

T, K	ρ, kg/m³	μ, Pa · s	ν, m²/s	c_p, kJ/(kg · K)	k, W/(m · K)	Pr
100	0.4878	97.80 −07	20.05 −06	5.194	73.60 −03	0.690
150	0.3252	12.50 −06	38.44 −06	5.194	96.90 −03	0.670
200	0.2439	15.10 −06	61.91 −06	5.193	11.80 −02	0.665
250	0.1951	17.60 −06	90.20 −06	5.193	13.70 −02	0.667
300	0.1626	19.90 −06	12.24 −05	5.193	15.50 −02	0.667
350	0.1394	22.20 −06	15.93 −05	5.193	17.20 −02	0.670
400	0.1220	24.30 −06	19.93 −05	5.193	18.90 −02	0.668
450	0.1084	26.40 −06	24.35 −05	5.193	20.50 −02	0.669
500	0.0976	28.40 −06	29.11 −05	5.193	22.10 −02	0.667
600	0.0813	32.20 −06	39.61 −05	5.193	25.10 −02	0.666
700	0.0697	35.90 −06	51.52 −05	5.193	28.00 −02	0.666
800	0.0610	39.40 −06	64.62 −05	5.193	30.70 −02	0.666
900	0.0542	42.80 −06	78.97 −05	5.193	33.40 −02	0.665
1,000	0.0488	46.20 −06	94.71 −05	5.193	36.00 −02	0.666
1,100	0.0445	49.40 −06	11.14 −04	5.193	38.50 −02	0.666
1,200	0.0407	52.50 −06	12.91 −04	5.193	41.00 −02	0.665
1,300	0.0375	55.60 −06	14.82 −04	5.193	43.40 −02	0.665
1,400	0.0348	58.60 −06	16.82 −04	5.193	45.70 −02	0.666

(Kays and London, 1984:284)

Properties of 304 Stainless Steel at 300K

ρ_s = 7900 kg/m^3

c_s = 477 J/kg·K

k_s = 14.9 W/m·K

(Incropera and DeWitt, 1990:A5)

Appendix B: N_{tu} vs. *maximum slope*

Table B.1 N_{tu} vs. *maximum slope*

N_{tu}	*maximum slope*	N_{tu}	*maximum slope*	N_{tu}	*maximum slope*
10	0.929	130	3.226	245	4.422
15	1.121	135	3.287	250	4.467
20	1.286	140	3.347	255	4.511
25	1.432	145	3.406	260	4.555
30	1.565	150	3.464	265	4.599
35	1.687	155	3.521	270	4.642
40	1.801	160	3.577	275	4.684
45	1.908	165	3.632	280	4.727
50	2.010	170	3.686	285	4.769
55	2.107	175	3.740	290	4.810
60	2.199	180	3.793	295	4.851
65	2.288	185	3.845	300	4.892
70	2.373	190	3.896	305	4.933
75	2.455	195	3.947	310	4.973
80	2.535	200	3.997	315	5.013
85	2.612	205	4.046	320	5.052
90	2.687	210	4.095	325	5.091
95	2.760	215	4.144	330	5.130
100	2.832	220	4.191	335	5.169
105	2.901	225	4.239	340	5.207
110	2.969	230	4.285	345	5.245
115	3.035	235	4.331	350	5.283
120	3.100	240	4.377	355	5.321
125	3.163				

Curve fits from the above table

$$N_{tu} = a(\textit{maximum slope})^{b} \qquad (2.12)$$

maximum slope	*a*	*b*
[0.92, 2.00)	11.77	2.084
[2.00, 2.80)	12.19	2.023
[2.80, 5.32)	12.38	2.008

Note: The QBasic program listing on the next page generated this table. It is based on Eq. 2.7.

```
REM This program finds the maximum slope of non-dimensional
temperature
REM for lamda =0 Note:  calculation of Bessel uses
logrithmns
DECLARE SUB bessel1 (x, I1#)
OPEN "blog1.dat" FOR OUTPUT AS #1
tau = .001: deltatau = .5
PRINT #1, "'Ntu'", "'maxslope'", "'tau'"
FOR Ntu = 10 TO 500 STEP 5
REM PRINT #1, "'Ntu ='", Ntu
slope2 = 0: slope1 = 0
DO UNTIL slope2 < slope1
        x = 2 * SQR(Ntu * tau)
REM        PRINT x
        bessel1 x, I1#: REM call the modified bessel
subroutine
        slope1 = slope2
        slope2 = Ntu ^ 2 / SQR(Ntu * tau) * I1# * EXP(-(Ntu
+ tau))
REM PRINT #1, tau, slope2
tau = tau + deltatau
REM PRINT slope2
        LOOP
PRINT #1, Ntu, slope1, tau
PRINT Ntu, slope1, tau
NEXT Ntu

CLOSE #1

SUB bessel1 (x, Inew#)
REM hyperbolic (modified) bessel function: n=1
REM using logrithms
lfact1# = 0: fact2# = 0
k = 1
Inew# = 0: Iold# = 1
DO UNTIL ABS(Iold# - Inew#) / Iold# < .000001
Iold# = Inew#
lfact1# = lfact2#:
lfact2# = lfact2# + LOG(k)
REM Inew# = Inew# + x ^ (1 + 2 * (k - 1)) / 2 ^ (1 + 2 * (k
- 1)) / fact1# / fact2#
lratio = (1 + 2 * (k - 1)) * LOG(x) - (1 + 2 * (k - 1)) *
LOG(2) - lfact1# - lfact2#
Inew# = Inew# + EXP(lratio)
IF k = 1 THEN Iold# = 1
k = k + 1
LOOP
END SUB
```

TABLE C.1

SCREEN PROPERTIES

mesh (in.$^{-1}$)	*R*	*d*† (mm)	*D* (mm)	*L* (mm)	W_s (kg)	*p*	A_c (10^{-4} m^2)	*A* (m^2)	Screen Count
250	0.000	0.041	14.96	37.3	0.01539*	0.7032	1.236	0.1917	429
250	0.143	0.041	14.96	36.8	0.016728	0.6730	1.183	0.2084	473
250	0.286	0.041	14.96	37.1	0.018820	0.6346	1.116	0.2345	568
250	0.486	0.041	14.96	37.1	0.025258	0.5095	0.8956	0.3147	764
325	0.000	0.036	14.96	36.6	0.016504	0.6751	1.187	0.2350	460
325	0.152	0.036	14.96	37.1	0.018766	0.6356	1.117	0.2672	515
325	0.303	0.036	14.96	37.1	0.021987	0.5731	1.007	0.3131	608
325	0.485	0.036	14.96	37.1	0.029637	0.4245	0.7462	0.4220	820
---	Empty	Tube	14.96	38.1	0.00	1.0000	1.758	0.00004	0

Note: † The manufacturer's wire diameters were listed as "0.0016 in." for 250 *mesh*, and 0.0014 in. for 325 *mesh*.
* The mass for this regenerator estimated using screen count and the average mass of 24 screens

TABLE D.1

RESULTS FOR 250 *mesh* R = 0.000

P_1 (MPa)	ΔP (kPa)	T_1 (K)	W (g/s)	Re	f	Re_d	C_D	$\left.\frac{dT^*}{d\theta}\right\|_{max}$ (s^{-1})	*maximum slope*	N_{tu}	j_H
1.014	8.41	294.4	0.281	11.1	3.47	9.18	3.36	0.4175	2.103	54.79	0.02697
1.013	60.75	294.5	1.151	45.6	1.45	37.62	1.40	2.348	2.884	103.84	0.05111
1.017	318.01	299.8	2.873	112.5	1.01	92.75	0.98	4.962	2.442	74.14	0.03649
2.023	4.46	292.4	0.282	11.2	3.68	9.26	3.56	0.4105	2.058	52.45	0.02582
2.016	20.42	295.3	0.854	33.8	1.81	27.85	1.75	1.688	2.796	97.50	0.04799
2.014	136.27	297.5	2.902	114.3	1.00	94.19	0.97	3.972	1.935	46.57	0.02292
3.039	2.75	292.7	0.282	11.2	3.41	9.24	3.30	0.3874	1.945	47.06	0.02316
3.041	13.39	294.5	0.855	33.9	1.79	27.95	1.73	1.963	3.245	131.58	0.06477
3.025	89.07	293.8	2.930	116.4	1.00	95.93	0.97	4.778	2.305	65.99	0.03248

TABLE D.2

RESULTS FOR 250 *mesh* $R = 0.143$

P_1 (MPa)	ΔP (kPa)	T_1 (K)	W (g/s)	Re	f	Re_d	C_D	$\left.\frac{dT^*}{d\theta}\right\|_{max}$ (s^{-1})	*maximum slope*	N_{Nu}	j_H
1.013	9.27	294.5	0.281	10.1	3.08	9.18	3.21	0.3141	1.719	36.39	0.01577
1.013	24.54	294.2	0.565	20.3	2.00	18.48	2.09	1.112	3.025	114.27	0.04952
1.011	67.79	294.4	1.153	41.5	1.29	37.70	1.35	2.102	2.801	97.89	0.04242
1.009	327.79	295.0	2.899	104.2	0.82	94.65	0.86	4.666	2.473	76.06	0.03296
2.028	4.67	292.1	0.282	10.2	3.11	9.27	3.24	0.3172	1.728	36.77	0.01594
2.026	12.18	293.3	0.566	20.4	2.00	18.55	2.09	1.051	2.854	101.64	0.04404
2.029	33.12	297.7	1.148	41.0	1.30	37.23	1.36	2.214	2.964	109.71	0.04754
2.012	145.70	294.7	2.921	105.1	0.86	95.44	0.89	4.198	2.208	60.49	0.02621
3.041	3.09	295.0	0.281	10.1	3.09	9.17	3.22	0.3421	1.872	43.46	0.01884
3.041	8.07	295.4	0.564	20.2	2.00	18.39	2.08	1.039	2.831	100.06	0.04336
3.040	22.48	293.4	1.158	41.8	1.32	37.95	1.38	1.958	2.598	84.04	0.03642
3.042	96.62	296.9	2.884	103.2	0.90	93.76	0.93	5.466	2.912	105.84	0.04587

TABLE D.3

RESULTS FOR 250 *mesh* R = 0.286

P_1 (MPa)	ΔP (kPa)	T_1 (K)	W (g/s)	Re	f	Re_d	C_D	$\left.\frac{dT^*}{d\theta}\right\|_{max}$ (s^{-1})	*maximum slope*	N_{tu}	j_H
1.013	11.69	293.3	0.281	9.08	2.90	9.21	3.36	0.2312	1.422	24.50	0.00890
1.015	30.33	294.3	0.564	18.18	1.84	18.46	2.14	0.9586	2.936	107.64	0.03911
1.015	84.39	294.7	1.149	36.98	1.20	37.54	1.39	2.169	3.263	133.04	0.04834
0.998	427.38	298.8	2.890	92.12	0.71	93.53	0.82	3.693	2.209	60.54	0.02200
2.025	5.93	293.0	0.281	9.08	2.95	9.22	3.42	0.2452	1.508	27.71	0.01007
2.028	15.42	293.8	0.565	18.22	1.89	18.50	2.19	0.9546	2.920	106.46	0.03868
2.027	41.35	294.5	1.150	37.04	1.21	37.60	1.41	2.097	3.151	124.05	0.04507
2.027	181.66	298.0	2.887	92.18	0.81	93.59	0.93	5.098	3.053	116.41	0.04229
3.039	3.90	293.1	0.281	9.09	2.91	9.23	3.37	0.2585	1.588	30.84	0.01121
3.042	10.00	294.3	0.564	18.18	1.85	18.45	2.14	0.9241	2.831	100.02	0.03634
3.041	27.45	295.3	1.150	36.95	1.21	37.51	1.41	2.148	3.229	130.30	0.04734
3.044	118.79	296.2	2.901	93.04	0.81	94.46	0.94	4.795	2.857	101.89	0.03702

TABLE D.4

RESULTS FOR 250 *mesh* R = 0.486

P_1 (MPa)	ΔP (kPa)	T_1 (K)	W (g/s)	Re	f	Re_d	C_D	$\left.\frac{dT^*}{d\theta}\right\|_{max}$ (s^{-1})	*maximum slope*	N_{tu}	j_H
1.013	33.27	292.2	0.282	6.81	3.13	9.27	6.77	0.1359	1.117	14.83	0.00322
1.013	89.44	294.1	0.566	13.59	2.02	18.51	4.37	0.6172	2.531	79.74	0.01732
1.015	262.33	294.9	1.151	27.59	1.28	37.59	2.76	1.665	3.356	140.74	0.03058
1.015	678.87	295.3	1.844	44.16	0.75	60.17	1.62	2.296	2.888	104.14	0.02263
2.027	16.62	292.2	0.282	6.81	3.17	9.27	6.86	0.1344	1.105	14.49	0.00315
2.028	43.74	293.5	0.566	13.61	2.05	18.55	4.43	0.6053	2.481	76.55	0.01663
2.029	117.61	294.7	1.151	27.60	1.30	37.60	2.82	1.62	3.266	133.27	0.02895
2.028	578.21	296.3	2.908	69.46	0.86	94.64	1.86	4.404	3.514	154.40	0.03354
3.040	11.07	292.9	0.282	6.79	3.17	9.25	6.85	0.1366	1.124	15.01	0.00326
3.042	28.89	294.0	0.566	13.60	2.04	18.53	4.41	0.6049	2.479	76.43	0.01660
3.042	78.46	295.6	1.151	27.53	1.32	37.51	2.86	1.539	3.103	120.30	0.02614
3.043	350.28	296.4	2.891	69.05	0.89	94.07	1.92	4.034	3.237	130.96	0.02845

TABLE D.5

RESULTS FOR 325 *mesh* R = 0.000

P_1 (MPa)	ΔP (kPa)	T_1 (K)	W (g/s)	Re	f	Re_d	C_D	$\left.\frac{dT^*}{d\theta}\right\|_{max}$ (s^{-1})	*maximum slope*	N_{tu}	j_H
1.013	12.46	292.2	0.282	8.99	3.69	9.83	3.25	0.3137	1.686	34.95	0.01347
1.014	31.93	294.0	0.566	17.95	2.32	19.63	2.04	1.111	2.977	110.66	0.04267
1.014	85.41	296.9	1.148	36.17	1.45	39.56	1.27	2.161	2.854	101.69	0.03921
1.015	423.66	298.2	2.890	90.80	0.87	99.33	0.76	5.151	2.702	90.98	0.03508
2.027	6.15	292.3	0.282	8.98	3.67	9.83	3.22	0.3142	1.689	35.07	0.01352
2.027	15.91	293.3	0.566	18.00	2.34	19.69	2.05	1.148	3.072	117.87	0.04545
2.028	41.69	297.2	1.147	36.10	1.47	39.49	1.29	2.597	3.434	147.40	0.05684
2.029	174.72	297.8	2.888	90.83	0.93	99.36	0.82	5.287	2.775	96.03	0.03703
3.040	4.34	292.3	0.282	8.99	3.88	9.83	3.41	0.3425	1.840	41.93	0.01617
3.040	10.52	294.9	0.565	17.89	2.32	19.57	2.04	1.145	3.072	117.85	0.04544
3.041	27.45	296.5	1.147	36.19	1.46	39.59	1.28	2.453	3.241	131.25	0.05061
3.043	114.39	299.4	2.879	90.20	0.94	98.67	0.83	4.847	2.552	81.07	0.03126

TABLE D.6

RESULTS FOR 325 *mesh* R = 0.152

P_1 (MPa)	ΔP (kPa)	T_1 (K)	W (g/s)	Re	f	Re_d	C_D	$\left.\frac{dT^*}{d\theta}\right\|_{max}$ (s^{-1})	*maximum slope*	N_{tu}	j_H
1.013	15.73	292.0	0.282	8.01	3.43	9.82	3.43	0.2145	1.312	20.74	0.00662
1.013	40.86	292.6	0.566	16.07	2.17	19.71	2.17	0.9053	2.756	94.75	0.03024
1.013	108.90	295.2	1.150	32.43	1.34	39.78	1.34	1.940	2.909	105.65	0.03372
1.014	524.32	297.9	2.776	77.83	0.76	95.48	0.76	4.031	2.503	77.94	0.02487
2.027	7.86	292.4	0.282	8.00	3.45	9.81	3.45	0.2199	1.346	21.86	0.00698
2.027	20.20	293.2	0.565	16.03	2.18	19.66	2.19	0.7964	2.428	73.29	0.02339
2.028	53.31	295.6	1.149	32.38	1.37	39.72	1.38	1.946	2.920	106.45	0.03397
2.028	223.57	299.5	2.879	80.41	0.86	98.65	0.87	3.783	2.265	63.68	0.02032
3.039	5.44	292.7	0.282	7.99	3.58	9.81	3.58	0.2461	1.506	27.62	0.00882
3.041	13.49	294.3	0.564	15.96	2.19	19.57	2.20	0.8706	2.659	88.09	0.02811
3.040	35.11	295.8	1.149	32.36	1.37	39.70	1.37	2.095	3.143	123.44	0.03939
3.045	144.72	298.8	2.880	80.57	0.87	98.84	0.87	3.803	2.276	64.33	0.02053

TABLE D.7

RESULTS FOR 325 *mesh* R = 0.303

P_1 (MPa)	ΔP (kPa)	T_1 (K)	W (g/s)	Re	f	Re_d	C_D	$\left.\frac{dT^*}{d\theta}\right\|_{max}$ (s^{-1})	*maximum slope*	N_{tu}	j_H
1.013	24.17	293.0	0.282	6.82	3.27	9.80	4.30	0.1807	1.295	20.17	0.00495
1.013	62.24	294.1	0.566	13.66	2.04	19.63	2.68	0.6874	2.453	74.86	0.01838
1.014	169.12	296.3	1.149	27.60	1.25	39.67	1.65	1.622	2.850	101.41	0.02490
1.015	606.00	298.2	2.336	55.85	0.68	80.29	0.90	3.224	2.787	96.89	0.02379
2.027	12.12	293.8	0.281	6.80	3.31	9.77	4.35	0.1715	1.231	18.14	0.00445
2.027	30.47	294.9	0.565	13.61	2.05	19.56	2.69	0.6258	2.238	62.15	0.01526
2.027	79.36	296.3	1.149	27.59	1.27	39.66	1.67	1.645	2.892	104.38	0.02563
2.028	348.92	298.9	2.885	68.87	0.81	99.00	1.06	3.292	2.304	65.95	0.01619
3.039	8.05	293.2	0.282	6.81	3.30	9.79	4.34	0.1586	1.137	15.38	0.00378
3.039	20.52	295.2	0.565	13.59	2.08	19.54	2.73	0.6529	2.335	67.75	0.01664
3.039	52.99	297.3	1.147	27.48	1.28	39.50	1.69	1.692	2.979	110.83	0.02721
3.041	220.98	298.8	2.884	68.84	0.82	98.97	1.08	3.293	2.306	66.06	0.01622

TABLE D.8

RESULTS FOR 325 *mesh* R = 0.485

P_1 (MPa)	ΔP (kPa)	T_1 (K)	W (g/s)	Re	f	Re_d	C_D	$\left.\frac{dT^*}{d\theta}\right\|_{max}$ (s^{-1})	*maximum slope*	N_{Nu}	j_H
1.014	91.46	293.7	0.281	5.03	3.62	9.75	11.66	0.1011	0.980	11.29	0.00152
1.013	257.59	294.0	0.564	10.11	2.26	19.59	7.28	0.5063	2.442	74.16	0.01001
1.013	784.53	296.9	0.982	17.46	0.97	33.84	3.12	1.250	3.467	150.24	0.02028
2.026	44.10	292.9	0.281	5.05	3.62	9.78	11.66	0.1013	0.981	11.30	0.00153
2.027	115.80	294.0	0.564	10.11	2.31	19.59	7.43	0.4684	2.259	63.35	0.00855
2.027	327.65	297.2	1.145	20.36	1.47	39.44	4.75	1.496	3.557	158.21	0.02136
2.029	---	297.4	2.424	43.08	----	83.46	---	3.454	3.879	188.27	0.02541
3.040	29.47	293.9	0.281	5.03	3.65	9.75	11.76	0.09604	0.931	10.14	0.00137
3.040	76.78	295.0	0.564	10.07	2.33	19.51	7.52	0.4695	2.268	63.85	0.00862
3.041	209.80	297.2	1.145	20.36	1.50	39.44	4.83	1.421	3.379	142.67	0.01926
3.042	950.68	298.2	2.884	51.15	0.90	99.10	2.90	3.860	3.644	166.08	0.02242

TABLE D.9

REPEAT RESULTS FOR 250 *mesh* R = 0.286 and EMPTY TUBE TESTS

P_1 (MPa)	ΔP (kPa)	T_1 (K)	W (g/s)	Re	f	Re_d	C_D	$\left.\frac{dT^*}{d\theta}\right\|_{max}$ (s^{-1})	*maximum slope*	N_{Nu}	j_H
Repeat											
2.027	5.85	292.2	0.283	9.14	2.90	---	---	0.2887	1.767	38.53	0.01400
2.026	15.59	294.5	0.565	18.18	1.91	---	---	0.9336	2.858	101.97	0.03705
2.027	40.84	294.6	1.153	37.12	1.19	---	---	2.030	3.043	115.67	0.04202
2.029	181.38	298.7	2.895	92.29	0.80	---	---	4.308	2.573	82.41	0.02994
Empty Tube											
1.013	0.017	292.9	0.281	---	---	---	---	---	---	---	---
1.015	-0.568	296.2	2.900	---	---	---	---	---	---	---	---
3.040	0.017	293.8	0.282	---	---	---	---	---	---	---	---
3.042	-0.251	296.9	2.898	---	---	---	---	---	---	---	---

Appendix E: Data Acquisition Program

```
'*****************************************************************
120 '  This is the temperature data collection program
140
'*****************************************************************
150 SCREEN 0,0,0: KEY OFF:CLS:WIDTH 80
160 CLEAR, 49152!
165 LOCATE 25,1:COLOR 0,7:PRINT"-PLEASE WAIT-";:COLOR
7,0:PRINT"  Loading DAS-8 I/O address and thermocouple
lookup table data":LOCATE 1,1
170 DEF SEG = 0
180 SG = 256 * PEEK(&H511) + PEEK(&H510)
190 SG = SG + 49152!/16
200 DEF SEG = SG
210 BLOAD "DAS8.BIN", 0
213 CLS
220 OPEN "DAS8.ADR" FOR INPUT AS #1
230 INPUT #1, BASADR%    'initialize & declare CALL
parameters
240 CLOSE #1
250 DAS8 = 0
260 FLAG% = 0
270 MD% = 0              'Mode 0 = initialization
280 CALL DAS8 (MD%, BASADR%, FLAG%)
290 IF FLAG% <>0 THEN PRINT"INSTALLATION ERROR"
292 'initialize variables
293 ZMAX%=500:ZM%=ZMAX%:DIM D%(2,ZM%),TIME(ZM%)
295 'Get gain setting of EXP-16
300 AV=1000:'CLS:INPUT "EXP-16 Gain setting (100,200,1000
etc.): ",AV
301 ' ------ control menu -------------
302 AGE$(0)="old":AGE$(1)="new"
305 KEY(1) ON
306 KEY(10) ON
310 ON KEY(1) GOSUB 2000
315 ON KEY(10) GOSUB 3000
320 IF JU =1 THEN CLS:JU=0
322 LOCATE 5,15
325 PRINT"filename:  ";N$,AGE$(WARN)
330 PRINT:PRINT"T(1) = ";T(0)
335 PRINT:PRINT"T(2) = ";T(1)
340 PRINT:PRINT"T(3) = ";T(2)
342 PRINT "CJC  = ";CJC+273.15
345 PRINT:PRINT:PRINT"      F1 -  enter new filename"
350 PRINT"      F10 -  collect data "
355 ZM%=1
360 GOSUB 600 ' cold juntion and data collection
363 Z%=1
```

```
365 GOSUB 820 ' convert data to temperature
370 GOTO 320
549 'I reduced the sized of D% and T from 15 to 2 for this
program
550 '---- STEP 2: Initialize an integer array D%(15) to
receive data ------
560 DIM D%(2)  '16 elements, one for each EXP-16 channel
570 'Also initialize a corresponding real array to receive
temperature data
580 DIM T(2)
590 '
600 '----- STEP 3: Get cold junction compensation
temperature -------------
610 'Output of CJC channel is scaled at 24.4mV/deg.C. This
corresponds to
620 '0.1 deg.C./bit. Dividing output in bits by 10 yields
degrees C.
630 '
640 'Lock DAS-8 to channel #7 (CJC channel selected) using
mode 1
650 MD%=1 : LT%(0)=7 : LT%(1) = 7
660 CALL DAS8 (MD%, LT%(0), FLAG%)
670 IF FLAG% <> 0 THEN PRINT "ERROR IN SETTING CJC CHANNEL"
: END
680 'Next get CJC data from this channel using Mode 4
690 MD% = 4 : CJ%= 0
700 CALL DAS8 (MD%, CJ%, FLAG%)
710 'Change output in bits to real temperature
720 CJC = CJ%/10
730 '----- STEP 4: Get the thermocouple data ---------------
---------------
740 CH% = 0
750 FOR Z% = 1 TO ZM%
755 TIME(Z%)=TIMER
760 GOSUB 1000
765 NEXT Z%
770 RETURN
790 '  CH% - specifies DAS-8 channel that EXP-16 is
connected to (0-7).
800 '  D%(15) - integer data array to receive data from
channels.
810 '
820 '----- STEP 5: Convert data to volts and calculate
temperature -------
830 'AV = Gain setting on Dipswitch of EXP-16 (change to
suit).
835 CJC = CJ%/10
840 FOR I = 0 TO 2
850 V = (D%(I,Z%)*5)/(AV*2048)
865 VJ=1000*V+.992+(CJC-25)*.040667 'rem jeff's curve fit
867 T(I)=273.15+(-.0142857+25.8333*VJ-.595235*VJ^2)' curve
fit temperature
```

```
880 NEXT I
890 RETURN
1000 '---- Subroutine to convert EXP-16 channels to number
of bits --------
1010 'First lock DAS-8 on the one channel that EXP-16 is
connected to.
1020 LT%(0) = CH% : LT%(1) = CH% : MD% = 1
1030 CALL DAS8 (MD%, LT%(0), FLAG%)
1040 IF FLAG% <> 0 THEN PRINT "ERROR IN SETTING CHANNEL" :
END
1050 'Next select each EXP-16 channel in turn and convert
it.
1060 'Digital outputs OP1-4 drive the EXP-16 sub-multiplexer
address, so use
1070 'mode 14 to set up the sub-multiplexer channel.
1080 FOR SUB% = 0 TO 2   'note use of integer index SUB%
1090 MD% = 14
1100 CALL DAS8 (MD%, SUB%, FLAG%)       'address set
1110 IF FLAG% <> 0 THEN PRINT "ERROR IN EXP-16 CHANNEL
NUMBER" : END
1140 MD% = 4  'do 1 A/D conversion
1150 CALL DAS8 (MD%, D%(SUB%,Z%), FLAG%)
1160 IF FLAG% <> 0 THEN PRINT "ERROR IN PERFORMING A/D
CONVERSION"
1180 NEXT SUB%
1190 'All done - return fron subroutine
1200 RETURN
1210 '
2000 '---- subroutine to enter filename
2002 IF WARN = 0 THEN 2010
2005 INPUT "are you sure? (y/n)";A$
2007 IF A$<>"Y" AND A$<>"y" THEN 2120
2008 CLOSE #1:CLOSE #2:CLOSE #3
2010 LOCATE 18,10
2015 INPUT"enter 'filename'.dat";N$
2020 NA$="a:"+N$+".dat"
2030 NB$="b:"+N$+".prn"
2040 NC$="\thermo\data\"+N$+".dat"
2050 OPEN NC$ FOR APPEND AS #1
2060 OPEN NB$ FOR APPEND AS #2
2070 OPEN NA$ FOR APPEND AS #3
2080 PRINT #1,"'filename = ";NC$
2090 PRINT #2,"'filename = ";NB$
2100 PRINT #3,"'filename = ";NA$
2110 WARN = 1
2115 JU=1
2120 RETURN
3000 ' ------- subroutine for data collection
3005 LOCATE 18,10
3010 IF WARN = 0 THEN JU=1:CLS:PRINT "You forgot to enter
new filename.": GOTO 3140
3015 KEY(1) STOP:KEY(10) STOP
```

```
3020 PRINT "collecting data... "
3030 ZM%=ZMAX%
3040 GOSUB 600 ' collect data
3042 PRINT "saving data ..."
3044 PRINT #1, "'z%'","'delta
t'","'Temp(1)'","'Temp(2)'","'Temp(3)'"
3045 FOR Z% = 1 TO ZM%
3047 GOSUB 820 ' calculate temperatures
3048 PRINT #1, Z%,TIME(Z%)-TIME(1),T(0),T(1),T(2)
3050 NEXT Z%
3052 CLOSE #1
3054 PRINT #2, "'z%'","'delta
t'","'Temp(1)'","'Temp(2)'","'Temp(3)'"
3055 FOR Z% = 1 TO ZM%
3057 GOSUB 820 ' calculate temperatures
3058 PRINT #2, Z%,TIME(Z%)-TIME(1),T(0),T(1),T(2)
3060 NEXT Z%
3062 CLOSE #2
3064 PRINT #3, "'z%'","'delta
t'","'Temp(1)'","'Temp(2)'","'Temp(3)'"
3065 FOR Z% = 1 TO ZM%
3067 GOSUB 820 ' calculate temperatures
3068 PRINT #3, Z%,TIME(Z%)-TIME(1),T(0),T(1),T(2)
3070 NEXT Z%
3072 CLOSE #3
3120 WARN = 0
3130 KEY(1) ON: KEY (10) ON
3135 JU=1
3140 CLOSE #1
3150 CLOSE #2
3160 CLOSE #3
3180 'ERASE D%,TIME
3190 'DIM D%(2,ZM%),TIME(ZM%+1)
3195 SUB%=0:I=0:ZM%=1:Z%=1
3200 RETURN
60000 END
```

Appendix F: Sample Data Collection Sheet

Temperature Results

Capt Jeffrey L. Wiese
AFIT/ENY/GAE93D

Date:_____
Time:_____

Test No. _____ Filename:_____ Disk No. _____

Mesh Size: 250 325 Percent Roll: 0 15 30 50
Tank Pressure (psig) _____ Room Temp ( ) _____

Barometric Pressure (mm Hg) _____

Target inlet Press (atm) 10 20 30

Target Voltage = {14.6962*(atm)-mm Hg*(0.019337)}/49.965 = _____

Actual Voltage _____ Actual Pressure (P_1) = _____

Differential Pressure

Actual Voltage _____ Actual ΔP = _____

Initial Temperatures (degrees C)

T_1 = _____ T_2 = _____ T_3 = _____

Flowmeter

Reading _____ P_{meter} (Volts) = _____ P_{meter} (Pa) = _____

W_{He} (kg/sec) = _____ Comments:

_____

_____

Calculated Results

QBasic File: _____ Grapher File: _____ Quattro Pro File: _____

Grapher max $\frac{dt^*}{d\theta}\left(\frac{1}{\text{sec}}\right)$ = _____ QPro max $\frac{dt^*}{d\theta}\left(\frac{1}{\text{sec}}\right)$ = _____

conversion factor -- $\frac{W_t c_t}{W_{He} c_p}$ = _____ max non-dim slope = _____ _____

Table N_{tu} = _____ + $\left(\frac{\text{_____} - \text{_____}}{\text{_____} - \text{_____}}\right)$(_____ - _____) = _____

A(m^2) = _____ A_c(m^2) = _____ D(m) = _____ L(m) = _____ p = _____

Re = _____ $StPr^{2/3} = N_u \frac{A_t}{A} 0.667^{2/3}$ = _____

Bibliography

Atrey, M. D., S. L. Bapat, and K. G. Narayankhedkar. "Theoretical Analysis and Performance Investigation of Stirling Cycle Regenerators," Cryogenics, 31: 1044-1052 (December 1991).

Beckwith Thomas G. Mechanical Measurements (Third Edition). Reading MA: Addison-Wesley Publishing Company, 1982.

Borland Internation Inc. Quattro Pro Special Edition Manual. Scotts Valley CA: Borland International Inc, 1991.

Chan, C. K., E. Tward and W. W. Burt. "Overview of Cryocooler Technologies for Space-Based Electronics and Sensors," Proceeding of the 1989 Cryogenic Engineering Conference. 1239-1250. New York: Plenum Press, 1990.

Chi, S. W. Heat Pipe Theory and Practice. Washington: Hemisphere Publishing Corporation, 1976.

Dally, James W. and others. Instrumentation for Engineering Measurements. New York: John Wiley & Sons, Inc., 1984.

Gary, John and Ray Radebaugh. "An Improved Numerical Model for Calculation of Regenerator Performance (Regen 3.1)," Proceedings of the Fourth Interagency Meeting on Cryocoolers. DTIC-91/003, 165-176. January 1991.

Incropera, Frank P. and David P. DeWitt. Introduction to Heat Transfer (Second Edition). New York: John Wiley & Sons, 1990.

Kays, W. M. and A. L. London. Compact Heat Exchangers (Third Edition). New York: McGraw-Hill Book Company, 1984.

Pucci, P. F., C. P. Howard and C. H. Piersall, Jr. "The Single-Blow Transient Testing Technique for Compact Heat Exchangers," Journal of Engineering for Power, 89: 29-40 (January 1967).

Radebaugh, Ray. Chemical Science and Technology Laboratory, National Institute of Standards and Technology, Boulder CO. Telephone interview. 01 February 1993.

Rawlins, Wayne C. The Measurement and Modeling of Regenerator Performance in an Orifice Pulse Tube Refrigerator. PhD thesis, University of Colorado, Boulder CO, 1992.

Strang, Gilbert. Linear Algebra and Its Applications (Third Edition). Fort Worth: Harcourt Brace Jovanovich College Publishers, 1988.

Tailor, P.R., K. G. Narayankedkar. "Optimum Charts for a Piston-Displacer Stirling Cryocooler," Proceeding of the 1989 Cryogenic Engineering Conference. 1239-1250. New York: Plenum Press, 1990.

Tong, L. S. and A. L. London. "Heat Transfer and Flow-Friction Characteristics of Woven-Screen and Crossed-Rod Matrixes," Transactions of the ASME, 79: 1558-1570 (October 1957).

Walker, Graham. Cryocoolers Part 2: Applications. New York: Plenum Press, 1983.

Vita

Captain Jeffrey L. Wiese was born on 24 February 1964 in Idaho Falls, Idaho. He grew up the son of a chemical engineer for a major oil company so he grew up in Idaho, Utah, Kansas, and Oklahoma. He graduated from Sooner High School in Bartlesville, Oklahoma in 1982 and attended Oklahoma State University on a five-year Air Force Reserve Officer Training Course Scholarship. On 9 May 1987 he graduated with a Bachelor of Science in Mechanical Engineering (Aerospace Option) and received a reserve commission in the USAF. He entered active duty on 15 March 1988 at Chanute AFB, Illinois where he attended the Aircraft Maintenance Officer Course. After graduation in August 1988 he was an aircraft maintenance officer in the 366th Tactical Fighter Wing at Mountain Home AFB, Idaho. He worked on F/EF-111A, F-15C/E and F-16C aircraft. His numerous positions culminated as maintenance officer, 390th Fighter Squadron (F-15C). He entered the Graduate School of Engineering, Air Force Institute of Technology, in May 1992. His next assignment is to Phillips Laboratory, Space Thermal Technologies Branch located in Albuquerque New Mexico.

Permanent Address: Box 3517

Estes Park, Colorado 80517-3517

REPORT DOCUMENTATION PAGE

Form Approved
OMB No 0704-0188

1. AGENCY USE ONLY (Leave blank)	2. REPORT DATE	3. REPORT TYPE AND DATES COVERED
	December 1993	Master's Thesis

4. TITLE AND SUBTITLE
EXPERIMENTAL ANALYSIS OF HEAT TRANSFER CHARACTERISTICS AND PRESSURE DROP THROUGH SCREEN REGENERATIVE HEAT EXCHANGERS

5. FUNDING NUMBERS

6. AUTHOR(S)
Jeffrey L. Wiese, Captain, USAF

7. PERFORMING ORGANIZATION NAME(S) AND ADDRESS(ES)
Air Force Institute of Technology, WPAFB OH 45433-6583

8. PERFORMING ORGANIZATION REPORT NUMBER
AFIT/GAE/ENY/93D-30

9. SPONSORING / MONITORING AGENCY NAME(S) AND ADDRESS(ES)
Mr. Robert M. Vacek
PL/VTPT
3550 Aberdeen Ave SE
Bldg 30117, Kirtland AFB NM 87117-5776
(505) 846-2686 DSN: 246-2686

10. SPONSORING / MONITORING AGENCY REPORT NUMBER

11. SUPPLEMENTARY NOTES

12a. DISTRIBUTION / AVAILABILITY STATEMENT
Approved for public release; distribution unlimited

12b. DISTRIBUTION CODE

13. ABSTRACT *(Maximum 200 words)*
This study investigated the effect on heat transfer and friction chatacteristics for screen regenerative heat exchangers with the screen thickness reduced by rolling. The experiments were performed on 250 and 325 mesh, 304 stainless steel screen using helium gas. Reynolds numbers, based on hydraulic radius, Re, were between 10 and 100. Both the Colburn factor, $StPr^{2/3}$, and friction factor, f, decreased as the screen thickness was reduced. A correlation was found for predicting friction factor, f. The drag coefficient per screen remained nearly unchanged for thicknesses reduced not more than 30 percent. The decrease in Colburn factor was significant for Re less than 40. For Re between 40 and 100 the decrease in Colburn factor was less than the experimental uncertainty.

14. SUBJECT TERMS
Regenerative Cooling, Regenerators, Cryogenic Engines, Screens (Woven Materials), Mesh, Stirling Cycle

15. NUMBER OF PAGES
118

16. PRICE CODE

17. SECURITY CLASSIFICATION OF REPORT	18. SECURITY CLASSIFICATION OF THIS PAGE	19. SECURITY CLASSIFICATION OF ABSTRACT	20. LIMITATION OF ABSTRACT
Unclassified	Unclassified	Unclassfied	UL